This document was prepared for the ETI by third parties under contract to the ETI. The ETI is making these documents and data available to the public to inform the debate on low carbon energy innovation and deployment.

Programme Area: Marine

Project: PerAWAT

Title: Development of a Computational Fluid Dynamics Model for an Open-Centre Tidal Current Turbine

Abstract:

This deliverable is the second deliverable in WG3 WP5, and is concerned with the CFD modelling of a high solidity open-centre turbine, using the same modelling methodology as deliverable WG3 WP5 D1. The work was undertaken in two phases; the development of a basic analytical model of a high solidity turbine, in order to support the design of a credible turbine rotor; and subsequently, the CFD analysis of this design, in order to produce results for the velocity field in the wake of the turbine.

Context:

The Performance Assessment of Wave and Tidal Array Systems (PerAWaT) project, launched in October 2009 with £8m of ETI investment. The project delivered validated, commercial software tools capable of significantly reducing the levels of uncertainty associated with predicting the energy yield of major wave and tidal stream energy arrays. It also produced information that will help reduce commercial risk of future large scale wave and tidal array developments.

PerAWaT MA1003

Development of a computational fluid dynamics model for an open-centre tidal current turbine

WG3 WP5 D2

Dr Gareth I Gretton

The University of Edinburgh

Version: 2.0

9th December 2011

Revision history

Version	Issue date	Summary
0.1	5th September 2011	Preliminary draft showing key technical results.
0.2	30th September 2011	Expanded draft, incorporating initial feedback from PerAWaT members during EWTEC conference and following the September technical meeting.
1.0	9th November 2011	First version for prospective submission to ETI, following review of previous version by GH.
1.1	4th December 2011	Minor amendments and additions to 1.0.
2.0	9th December 2011	First version for submission to ETI, following approval of 1.1 by GH.

Executive summary

This report documents the work done for and represents deliverable two of WG3 WP5 (device scale numerical modelling: detailed CFD of other concepts). Deliverable two is concerned with the CFD modelling of a high solidity open-centre turbine, using the same modelling methodology as deliverable one. Two key phases of work were undertaken: the development of a basic analytical model of a high solidity turbine, in order to support the design of a credible turbine rotor; and subsequently, the CFD analysis of this design, in order to produce results for the velocity field in the wake of the turbine.

The basic analytical model combines the theory for the analysis of high-solidity turbomachines with actuator disc theory, along the lines of the classic blade element momentum theory for low solidity turbines. This allows for the specification of blade angles which should result in good turbine performance at the design tip speed ratio. It is shown that high solidity turbines will produce a thrust coefficient which decreases monotonically with an increase in the tip speed ratio; the opposite qualitative behaviour to that generally observed for low solidity turbines. The underlying reasons for this are explained in the report. Further preliminary work includes basic structural calculations and a consideration of the effect of ducting the high solidity turbine, based on results from WG3 WP1.

The second phase of work is the development of the CFD model. This uses the same modelling methodology as was used for the low solidity 'generic rotor' of deliverable one. Results from this confirm the prediction that high solidity turbines do show a decrease in the thrust coefficient with an increase in the tip speed ratio. The predicted power coefficient is seen to be lower than that seen for the generic rotor, but nevertheless potentially viable. Longitudinal and lateral profiles of the streamwise velocity in the wake are presented in the same format as in the deliverable one report. From these it is seen that the wake deficit is lower than that seen for the generic rotor, due to the lower thrust coefficients. It is also seen that the structure is notably different, this being primarily due to the 'internal' bypass flow that the open-centre of the turbine allows for.

Contents

1 Introduction and context

Deliverable two of WG3 WP5 (device scale numerical modelling: detailed CFD of other concepts) is concerned with the computational fluid dynamics modelling of an open-centre axial-flow turbine. As with deliverable one, the objective is to construct a numerical model that can be used as a *tool* to investigate and parameterize the wake behind the turbine. Furthermore, as this numerical model will be based on the same methodology as for the generic axial-flow turbine of D1, we will for the first time be able to provide an equitable comparison of the two technologies.

The starting point for the work on this deliverable was the specification of the geometry. It had been hoped that this could be obtained from OpenHydro, but this proved not to be possible and so it was required to develop a design as part of this deliverable. It was felt important that the design needed to be credible, by which it is meant that good hydrodynamic performance is achieved, in order to make the comparison with the generic turbine of D1 meaningful. In other words, as the design of the generic turbine is representative of good designs for that type of turbine, the open-centre turbine design must also be a good design.

Discussions were had within the consortium concerning the basic design parameters such as the turbine solidity. Clearly the specification of an open-centre axial-flow device does not fix the solidity, and examples of both high solidity (OpenHydro) and low solidity (Clean Current) open-centre devices exist. The decision to opt for a high solidity design was based on the implication that this would be the case in both the technology contract and WG0 D2. There was also the requirement to develop a design for the generator housing at the outer radius of the rotor, and this was again discussed within the consortium. It was decided here to use a duct for the generator housing, specifically 'duct H' from the work in WG3 WP1. This offered two key advantages: first, data exists from WG3 WP1 on the performance of duct H with an actuator disc representation of the turbine; and second, later work in WG3 WP1 will consider the performance of a low solidity axial-flow turbine within this same duct geometry, thereby allowing a more direct comparison between the performance of the different rotors considered in PerAWaT.

The design work on the open-centre rotor is presented in Section 2. As discussed there, a number of different modelling approaches were taken, namely: the use of basic axial-flow turbomachine theory (velocity triangles); the use of more advanced theory for a linear cascade;

and the consideration of the turbine as a series of blades in isolation (the approach used for low solidity turbines). The analysis based on velocity triangles was also extended by coupling this with actuator disc theory along the same lines as classic blade element momentum theory, and this modelling approach was ultimately used to define the open-centre rotor design. The effects of ducting are also outlined in this section (based on results from WG3 WP1), as well as a basic structural analysis used to determine a nominal blade thickness.

Following the specification of the rotor and duct geometry, Section 3 proceeds to the CFD analysis of the open-centre device. As noted there, this follows the same modelling methodology as was used for the generic turbine of D1. The grid setup is also highly similar, with comparable spacings normal to the wall, and comparable cell counts chordwise and spanwise on the turbine blade and also in the wake. This obviates the need for a repetition of the grid convergence studies of D1. Verification of the iterative convergence is, however, repeated. Following this, the model is used to investigate the effect of the tip speed ratio on a number of quantities, as with the study of the generic rotor in the D1 report. These quantities are the power and thrust coefficients, and longitudinal and lateral profiles of the velocities in the wake of the turbine. In addition, the pressure profiles on the blades at mid-span are also examined.

With respect to other deliverables in the present work package, and other work packages within the PerAWaT project, linkages are similar to that for D1 of this work package. Reference is therefore made to the discussion in the introduction to the D1 report. A synopsis of the deliverables in the present work package is given in Table 1 for context.

Table 1: *Synopsis of the deliverables for WG3 WP5.*

Deliverable	Objective
1	Construct a numerical model of a horizontal axis turbine.
2	Construct a numerical model of an open-centre turbine.
3	Parameterize the wake of the above two turbines, using the models developed.
4	Extend the models of D1 and D2 to incorporate unsteady upstream flow and update the parameterization.

2 Basic analysis and design of the turbine

2.1 Preliminary remarks

Prior to conducting a CFD analysis, a geometry for the open-centre rotor must be arrived at by recourse to basic fluid dynamics theory. This design process is described in the present section, which further includes a consideration of the effect of ducting and the results from a basic structural analysis, in order to determine a realistic blade thickness.

As discussed in the introduction, the intention is that this open-centre rotor will be of high solidity and that it will be representative[1] of the designs proposed by OpenHydro. A cursory inspection of photos on the OpenHydro website suggests that the solidity, defined as the chord over the stagger spacing[2], is approximately one.

A second aspect of this design is that the blades must be un-cambered as it is taken that there will be no pitching mechanism, nor indeed a yawing mechanism (which would be impractical). Further, it is taken that the blade profile is simply that of a flat plate.

Discussion within the consortium revealed that there was no 'accepted' design method for this type of turbine, although it is clear that the actuator disc concept is relevant. Three approaches were investigated as part of the present work: first, the standard analysis method for axial-flow turbomachines of high solidity, based on a consideration of the velocity triangles at inlet and exit to the cascade; second, the use of relations for a linear cascade (this method being related to the first); and third, the basic approach used for low solidity (wind and tidal current) turbines whereby blade section data for isolated aero/hydrofoils are used. The first method was also extended by coupling this with actuator disc theory along the same lines as classic blade element momentum theory.

This first method, in its simplest form, assumes that the blades used are able to turn the flow by the desired amount, and so no blade data is required. Typically (indeed universally) cambered blades are used and the 'design point' normally occurs where the flow enters and exits a blade passage in line with the blades. For the present turbine it has already been noted that the blades are limited to being un-cambered; thus, the problem reduces to specifying an appropriate angle

[1] *Representative* implies that the design developed herein is based on the same outline choices as are assumed to have been applied by OpenHydro in the development of their design; nevertheless as the blade design is based on first principles, it will be fundamentally generic.

[2] $\sigma = c/s$. This will be equivalent to planform blade area divided by the frontal area of the rotor

of incidence on to the blade, along with the rotational speed of the rotor. (An appropriate angle of incidence is one where the blades are not stalled and therefore the turbine will operate with relatively high efficiency.) As discussed subsequently, this method was used as the basis for the open-centre rotor design.

2.2 Nomenclature

Table 2: *Nomenclature for the basic hydrodynamic analysis of the turbine.*

Roman symbols	
a	Axial induction factor
A_{ref}	Reference area used when calculating C_P and C_T. Unless otherwise noted the reference area is that of the disc/rotor for a bare turbine and that of the duct for a ducted turbine.
c	Chord length
c_t	Coefficient giving flow deviation for a cascade
C_P	Power coefficient for the turbine, C_P = power/$(0.5\rho U_\infty^3 A_{\text{ref}})$.
C_T	Thrust coefficient for the turbine, C_T = axial force/$(0.5\rho U_\infty^2 A_{\text{ref}})$.
g	Acceleration due to gravity
H	Total head change across rotor
m	Gradient of the lift-curve slope
r_i	Turbine blade inner radius
r_o	Turbine blade outer radius
s	Stagger spacing
u	Blade velocity
U_∞	Flow velocity upstream of turbine
v_a	Axial flow velocity
V	Absolute velocity
w	Relative velocity
w_∞	Vector average of the inlet and outlet relative velocities
Greek symbols	
α	Angle between the absolute velocity (V) and the blade velocity (u). α_1 is at the entry to the blade row while α_2 is at the exit. (Note that α here is *not* the angle of attack.)

Continued on next page

α'	Angle of attack, as measured between the relative velocity at inlet (w_1) and the angle of zero lift (β_v)
$\alpha*$	Angle of attack, as measured between the vector average of the inlet and outlet relative velocities (w_∞) and the angle of zero lift (β_v)
β	Angle between the relative velocity (w) and the blade velocity (u). Subscripts 1 and 2 as per α.
β_v	Angle of zero lift
β_∞	Angle between the vector average of the inlet and outlet relative velocities (w_∞) and the blade velocity (u)
γ	Stagger angle
λ'	Blade speed ratio = u/U_∞
ρ	Fluid density
σ	Solidity = c/s
ϕ	Flow coefficient = v_a/u
Ψ	Head coefficient = gH/u^2

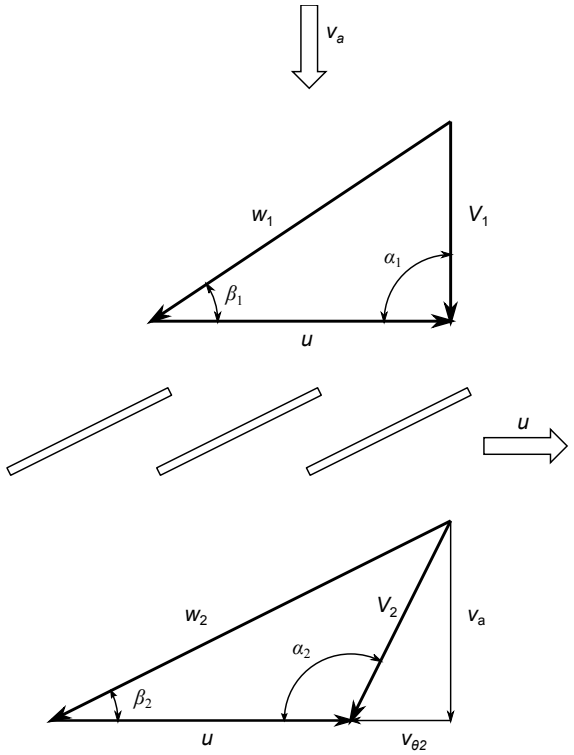

Figure 1: *Indicative velocity triangles at the inlet and outlet of a blade row.*

2.3 Hydrodynamic analysis as an axial-flow turbomachine

As noted above, for an axial-flow turbomachine with un-cambered blades the key design parameter is the angle of incidence (α') on the blade (in addition of course to the rotational speed of the turbine). Some insight into the values which can be achieved for a cascade are therefore required, as well as an indication of whether a turbine of solidity $\sigma = 1$ is within the gamut of a 'conventional' axial-flow turbomachine, and for which the deviation in the flow from the trailing edge of the blade is relatively small. If this deviation is small then the angle of incidence will be equal to the turning angle in the relative frame.

For the angle of attack, no definitive value was found for a flat plate cascade, but results in Johnson and Bullock (1965) (a seminal work on axial-flow compressors) and Japikse and Baines (1994) suggest that values less than 10° are typically used for cascades of aerofoils. This is comparable to the value of the angle of attack which might be specified for an isolated aerofoil, and therefore it is assumed that an effective angle of attack for an isolated foil (or flat plate) is appropriate for a cascade of those profiles. Section performance data for an isolated flat plate were found in Fage and Johansen (1927) (referenced by Hoerner, 1985) for angles of attack of 0°, 3°, 6°, 9°, 15°, and 20°, and increments of 10° upwards to 90°. These data indicate that lift stall occurs between 9° and 15°, but that the maximum lift to drag ratio (for the results given) occurs for an angle of attack of 3° – significantly lower than for common aerofoil sections. Based on these results then, it is believed that relatively low angles of attack, perhaps up to a maximum of 4° or 5° would be appropriate for the high solidity turbine design under consideration.

In respect of the solidity, Sabersky et al. (1999) report work on a linear cascade based on potential flow theory which shows that for $\sigma < 0.35$ the blades behave as isolated aerofoils while for $\sigma > 1$ the flow will exit the blade passage in line with the blades.[3] Johnson and Bullock (1965) also report experimental results for cascades with solidities ranging from 0.4 to 2.0, suggesting that a solidity of 1.0 is within the range used for 'conventional' axial-flow turbomachines.

We now proceed to a discussion of the basic analytical model developed (based on velocity triangles, and assuming no deflection), and the results produced. As with all of the other ana-

[3] Sabersky et al. state that the flow exits the blade passage in line with the blades for $\sigma > 2$ but this is at odds with the figure. An earlier (but still secondary) reference, (Wislicenus, 1947) states that the limiting value is indeed $\sigma = 1$.

lytical models discussed in this section, it is one-dimensional and therefore only considers the flow at a given radius (such that the blade speed ratio takes a single value); circumferential homogeneity is also assumed.

2.3.1 The influence of turning angle α' and blade speed ratio λ'

As a first step, we investigate the dependence of the thrust coefficient on the turning angle of the fluid (in the rotating frame) and the blade speed ratio. Turning angles of between 1° and 5° are investigated as these represent practical angles of incidence. In this model we assume that there is no feedback between the turbine and the flow, such that the axial speed through the turbine (v_a) is equal to the freestream speed.

The results of this model are shown in Figure 2. Clearly an increase in either the turning angle or the tip speed ratio increases the thrust coefficient, as would be expected. It is also seen that it is possible to achieve thrust coefficients in the desired range (the optimum for an actuator disc is 0.889), although, as noted, there is no flow-feedback in the current model and so the thrust coefficients predicted here are not directly comparable. Finally, an important point is that the thrust coefficient appears to increase exponentially, such that for the larger turning angles a small change in the blade speed ratio can cause a large increase in the thrust coefficient.

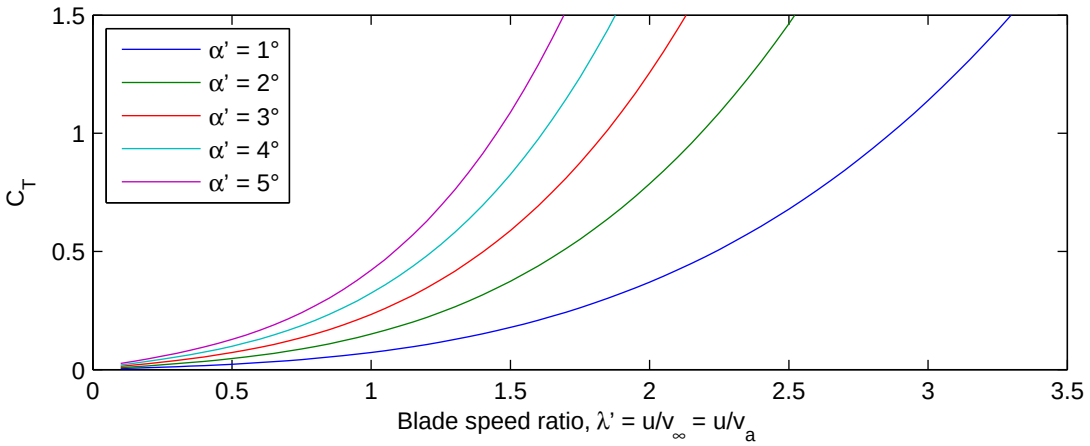

Figure 2: *Thrust coefficient versus blade speed ratio for five different turning angles.*

2.3.2 The influence of turning angle α' and blade speed ratio λ' with flow-feedback

As an evolution of the model discussed above, we now introduce flow-feedback using the actuator disc concept, including an empirical model for the behaviour at high thrust coefficients as per Burton et al. (2001). We again investigate the dependence of the thrust coefficient on the turning angle and the blade speed ratio.

The variation now seen for the thrust coefficient with the turning angle and blade speed ratio (Figure 3) is effectively shifted towards lower blade speed ratios, due to the effect of flow retardation at the actuator disc. Importantly, it is also difficult to find solutions for thrust coefficients above about 0.7, due to a positive feedback effect.[4] For example, for a turning angle of 3° a converged solution is found for a blade speed ratio of 1.5. If the turning angle is now increased, this will increase C_T and cause a consequent increase in the blade speed ratio (due to flow retardation). This then further increases C_T, continuing the increase in the blade speed ratio, and thus no solution is found.

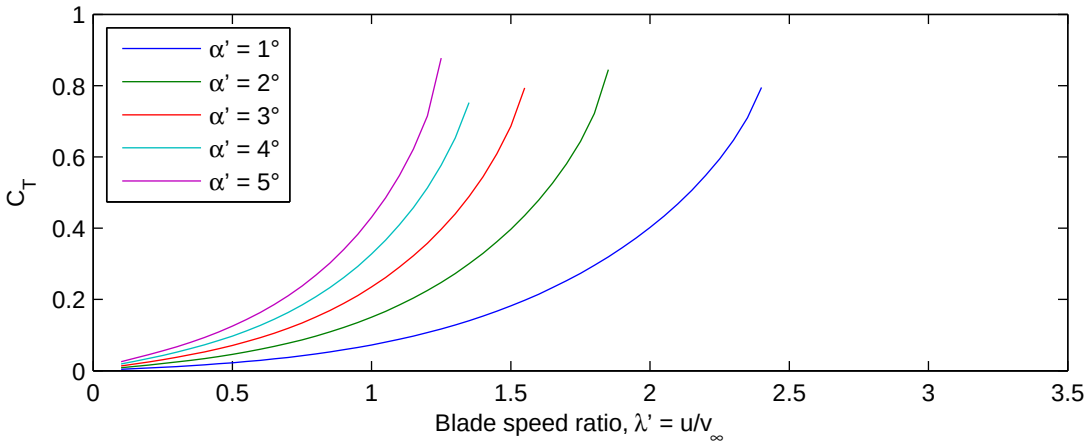

Figure 3: *Thrust coefficient versus blade speed ratio for five different turning angles.*

It might be taken that this implies that turbine operation will be unstable, but this is not necessarily the case. In the example here we are controlling the turning angle, which is effectively an output parameter, whereas in reality we would control the blade angle. The variation in the exit flow angle, which will be equal to the blade angle for high solidity, is shown in Figure 4. If we take it that the blade angle is fixed to, say, 30°, then as the blade speed ratio increases the angle of incidence will decrease. For low blade speed ratios, we will have high angles of incidence and the blades will likely stall, while for high blade speed ratios, the angle of incidence

[4] Solutions will exist, but they will be very sensitive to the turning angle and blade speed ratio

will reduce to zero and then become negative. A negative angle of incidence would then mean that the turbine had become a pump. Clearly the point of maximum power production will be between these two points, potentially within a relatively narrow range of the blade speed ratio.

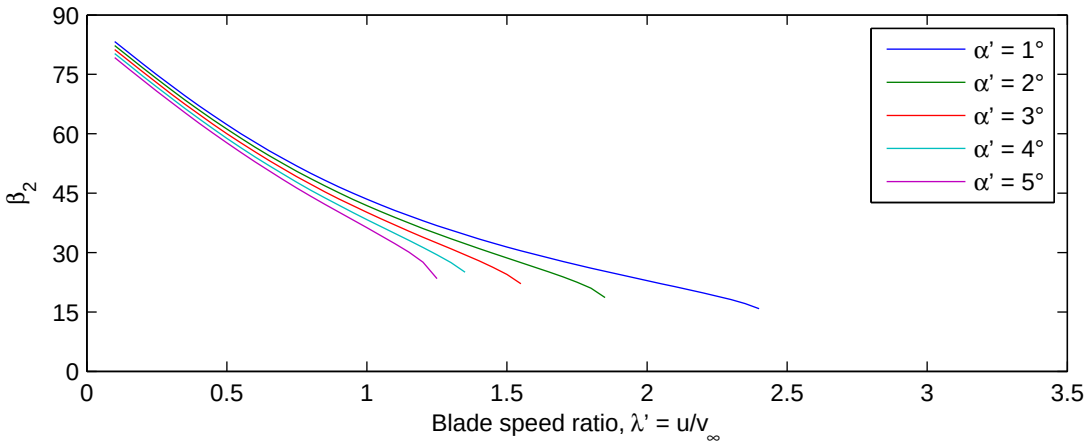

Figure 4: *Exit flow angle versus blade speed ratio for five different turning angles.*

2.3.3 The influence of blade speed ratio λ' for a series of blade angles

Using the model of the section above, we now investigate the behaviour of the turbine for a series of fixed exit flow angles, allowing the angle of incidence and therefore turning angle to vary as appropriate. Figure 5 shows the variation for the thrust coefficient, while Figure 6 shows the accompanying variation in the angle of incidence. The results are limited by the positive feedback discussed above, whereby a solution tends to increasing (and non-physical) values of the axial induction factor, and also for solutions which indicate an angle of incidence above 5° (these occurring for low tip speed ratios), above which angle separation would be expected to dominate, rendering the current, basic, model inappropriate.

It may be immediately highlighted that Figure 5 shows that the thrust coefficient decreases with an increase in the blade speed ratio, irrespective of the blade angle. This is as expected, based on the results of the previous graphs, but is the opposite to the trend generally seen for low solidity turbines.

The observed trend is explained by reference to Figure 7, which shows velocity vector triangles at entry to and exit from the blade row for three different blade speed ratios. (Please refer to Figure 1 for the notation.) The blade angle is equal to $26.6° = \arctan(1/2)$, which means that at

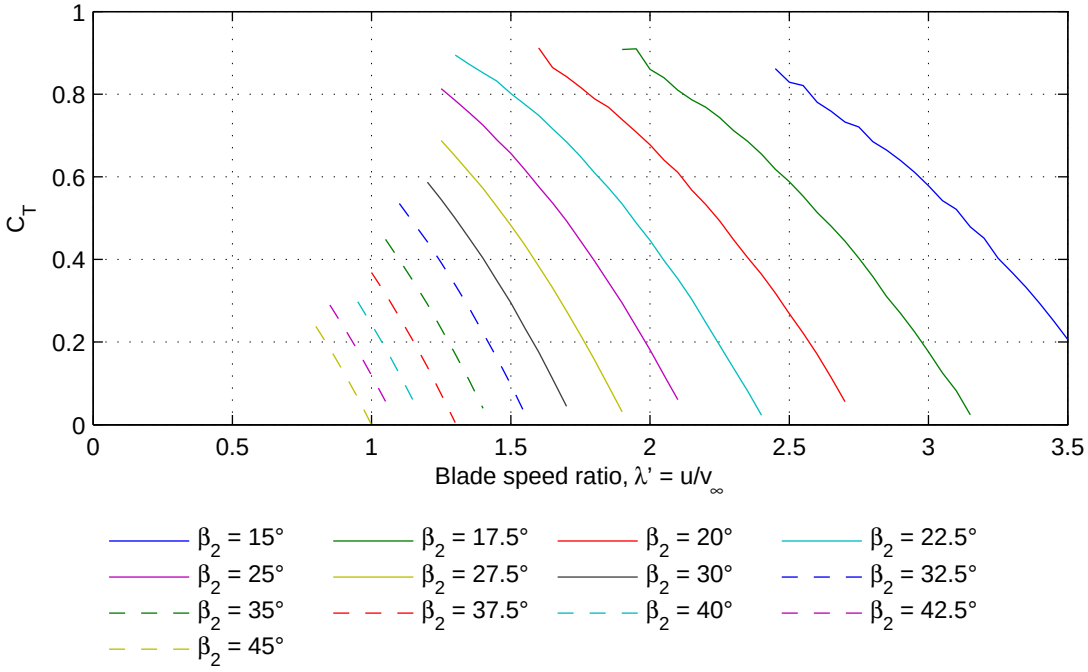

Figure 5: *Thrust coefficient versus blade speed ratio for a number of exit flow angles.*

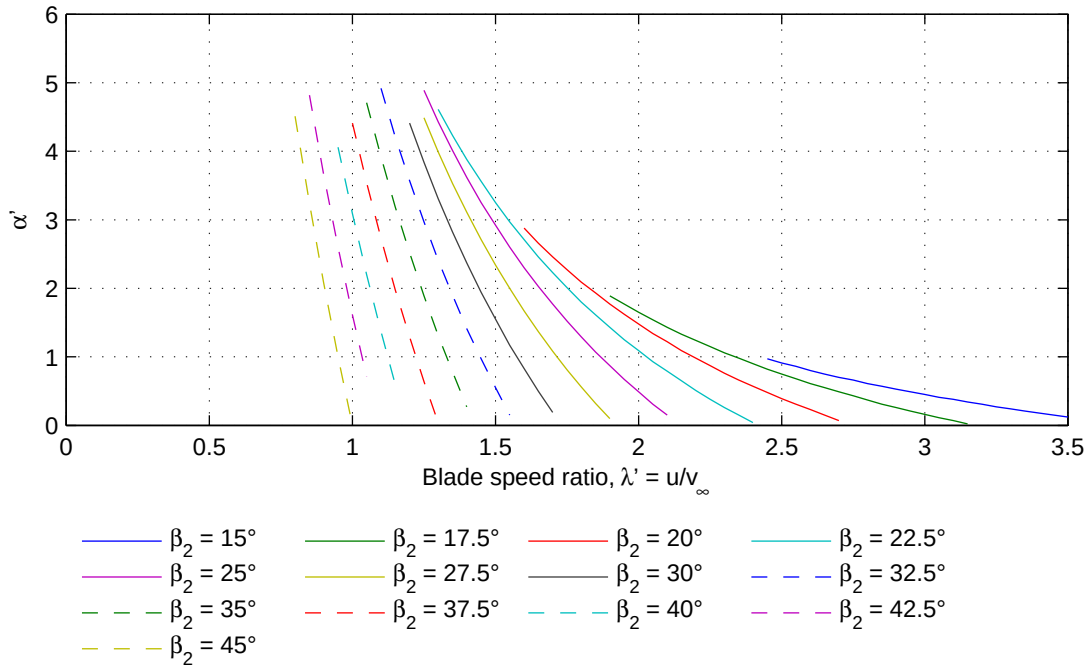

Figure 6: *Angle of incidence versus blade speed ratio for a number of exit flow angles.*

a blade speed ratio of 2.0 the angle of incidence will be zero, the entry and exit velocity triangles will be the same, and the turbine will produce no torque or thrust. For lower blade speed ratios, the angle of attack increases, thereby increasing the swirl (turning) generated by the turbine, this assuming that the flow remains attached. As the amount of swirl increases, the amount of torque generated increases, as does the absolute velocity at exit, which in turn increases the pressure drop across the turbine and therefore the thrust. In respect of the observed trend in C_T, it is also important to point out that a key assumption (that is approximately the case in practice) is that for high solidity turbines there is no circumferential variation in the velocity field; thus a high solidity turbine will turn all of the fluid passing through the rotor plane by the same amount (for a given case), as outlined.

For a low solidity turbine, the amount by which the fluid approaching the turbine is turned by the blades depends primarily on the lift force generated by the blades, as given by:

$$\text{Lift/unit span} = c_l \frac{1}{2} \rho W^2 c S \tag{1}$$

where c_l is the lift coefficient (approximately equal to $2\pi \sin \alpha'$ for low angles of attack), ρ is the fluid density, W is the relative flow velocity (approximately equal to the blade speed), and c is the chord. Thus, the turning achieved depends on the angle of attack *and* the blade speed ratio; specifically, it will vary linearly with the angle of attack but quadratically with the blade speed. Thus, as the blade speed ratio increases, the decrease in turning resulting from the decrease in the angle of attack is more than offset by the increase in turning resulting from the increase in the blade speed itself.

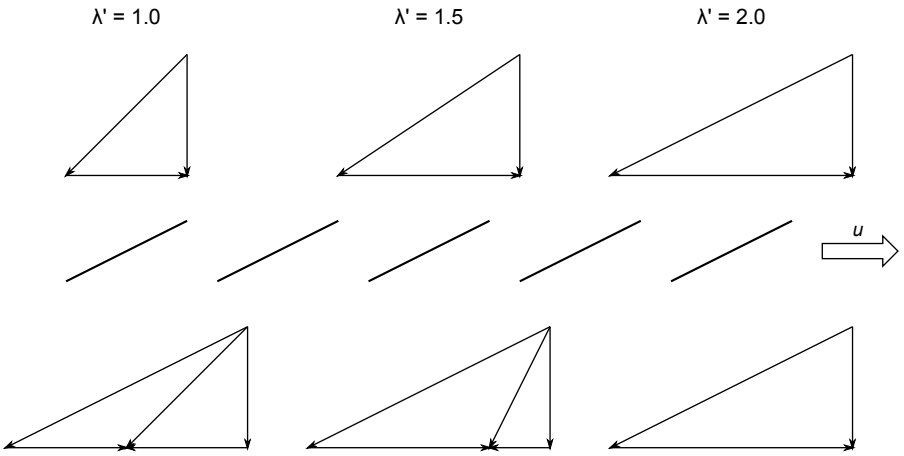

Figure 7: *Velocity vector diagrams for three different blade speed ratios, as indicated.*

Figure 5 also indicates that the range of blade speed ratios for which solutions exist (given the constraints of the model discussed above) becomes small for large exit flow angles ($\beta_2 \geq 45°$). For smaller exit flow angles, the 'working' range of tip speed ratio becomes approximately constant when the limiting factor at the lower tip speed ratio end of the curve is the high axial induction factor. This latter behaviour is explained by Figure 6 which shows that the variation in the angle of incidence with blade speed ratio becomes weaker (i.e. smaller change in α' for a given change in λ') for the smaller blade angles, which are more appropriate for operation at higher blade speed ratios.

2.3.4 Interim conclusions

The modelling discussed in this section provides valuable insight into the operation of a high solidity turbine, assuming that it behaves as a conventional axial-flow turbomachine. This is likely to be an accurate representation for the angles of attack considered (up to 5°) and where secondary effects, such as separation and flow deviation at the trailing edges of the blades, should not be dominant.

Thus, based on the above results it is suggested that a practical open-centre design, where the ratio r_o/r_i is 2, would have a design point blade speed ratio varying from 1.25 at the inner radius to 2.5 at the outer radius. The blade angle would vary from 32° at the inner radius to 17° at the outer radius, in order to achieve thrust coefficients between 0.4 at the inner radius and 0.6 at the outer radius. These values are chosen by inspection of Figure 5 and are intended to lie in the middle of the 'parameter space' represented on this figure. Specifically, this gives some margin from incidence angles which would be likely to lead to stall and operating points where the axial induction factor would increase sharply. Significantly higher thrust coefficients may be able to be attained in practice by dropping the rotational speed such that the blade speed ratio varies from 1.1 to 2.2, this giving thrust coefficients between around 0.5 and 0.75. As noted, this will be limited by the blades stalling, the limit of which is not known *a priori*. Conversely, increasing the rotational speed to give blade speed ratios in the range 1.5 to 3 would suggest thrust coefficients between 0.1 and 0.2.

As a final point of note, it may be reiterated that for small values of the exit flow angle the range of angle of incidence becomes small – indeed, no converged solution was obtained for an exit flow angle of 10°. This suggests that the range of practical blade speed ratios is broadly limited

to the range suggested above, with values outside of this producing either too high angles of incidence for low blade speed ratios (and thereby stalled blades) or too small a functional range of the angle of incidence for high blade speed ratios (meaning that the turbine has a very narrow operating range).

2.4 Hydrodynamic analysis as a linear cascade

In addition to the basic theory for turbomachines used above, Sabersky et al. (1999) also present formulae for the performance of a linear cascade of arbitrary solidity, this offering a potentially more accurate analysis. These formulae are written in terms of two non-dimensional coefficients, namely the total head coefficient:

$$\Psi = \frac{gH}{u^2} \tag{2}$$

and the flow coefficient:

$$\phi = \frac{v_a}{u} \tag{3}$$

The total head coefficient contributes to the thrust coefficient but is more compact to write, while the flow coefficient represents the inverse of the local blade speed ratio. We continue here with these standard expressions used in high solidity turbomachinery.

Assuming no deviation from the trailing edge of the blades, the total head change would be given by:

$$\Psi = 1 - \phi(\cot\beta_2 + \cot\alpha_1) \tag{4}$$

For a cascade of arbitrary solidity we have instead the following expression:

$$\Psi = c_t[1 - \phi(\cot\beta_v + \cot\alpha_1)] \tag{5}$$

which features the coefficient c_t, and a change from β_2 to β_v within the expression.

The coefficient c_t is defined as:

$$c_t = \frac{2m\sigma\sin\beta_v}{4 + m\sigma\sin\beta_v} \tag{6}$$

and where m, which represents the gradient of the lift-curve slope for the cascade, must be found from experiment or estimated from theory. For a flat plate cascade, and where the solidity is

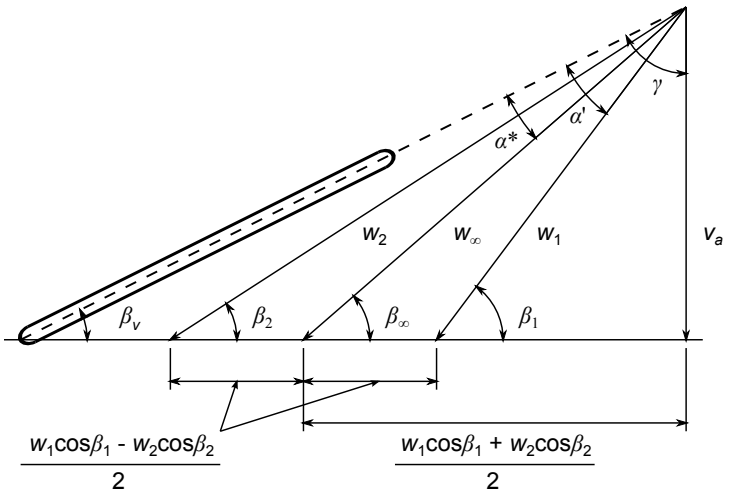

Figure 8: *Vane and flow angles for a linear cascade. Note that the blades are un-cambered flat plates, as per the present case, and that an arbitrary amount of flow deviation is shown in order to make the diagram clearer.*

low, typically less than 0.35, we can use the theoretical value for an isolated flat plate, namely $m = 2\pi$.

The coefficient c_t can also be written as:

$$c_t = \frac{\cot\beta_1 - \cot\beta_2}{\cot\beta_1 - \cot\beta_v} \tag{7}$$

This reveals that the physical meaning of c_t is the ratio of the change in tangential velocity achieved by the cascade to the change that would be achieved with no deviation from the blade angle β_v.

Results produced using the above theory, and assuming $m = 2\pi$ throughout, are shown in Figures 9 and 10, the former figure showing the variation in C_T with blade speed ratio for a number of solidities and the latter showing the variation in the coefficient c_t with solidity for a number of blade speed ratios. All of these results assume no flow-feedback.

Also shown in Figure 9 is a comparable result from the basic analysis (Section 2.3.1/Figure 2), labelled as '$\sigma = \infty$'. It is labelled as such because a notionally infinite solidity would result in no flow deviation. This comparison is indicative because of the differing assumptions in the two models.

For the range of thrust coefficients and blade speed ratios of interest it is clear that there is

broad agreement between the results for high solidity ($\sigma > 1$) and the result assuming no flow deviation. For high solidity and low blade speed ratio it is seen that values for c_t greater than unity are predicted, this leading to some of the finite solidity cases showing higher values of the thrust coefficient than the notionally infinite solidity case. This non-physical result is readily explained by the assumption that $m = 2\pi$ for all solidities (with the linear cascade model).

Overall, these results for a linear cascade add confidence that the departure from the idealized result (of no flow deviation) for a turbine of solidity of one will be relatively small.

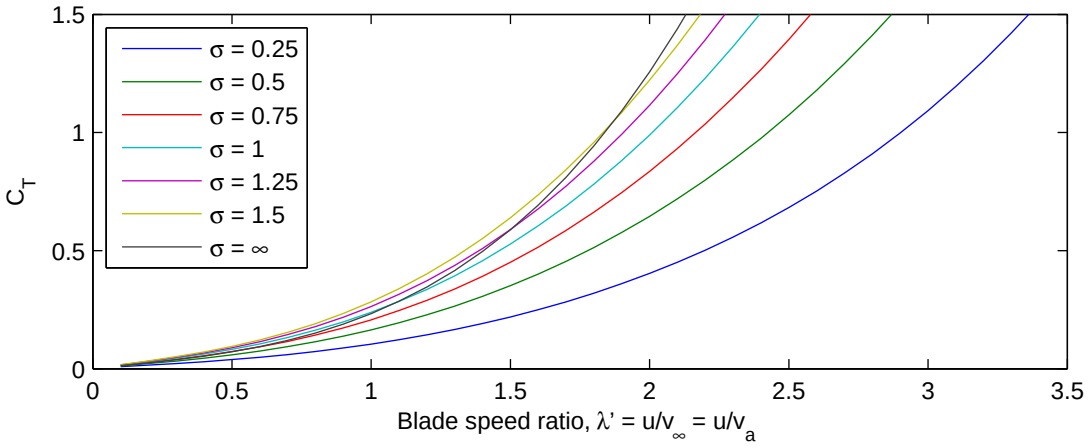

Figure 9: *Thrust coefficient versus blade speed ratio with varying solidity for $\alpha' = 3°$. $\sigma = \infty$ indicates the result which assumes no flow deviation.*

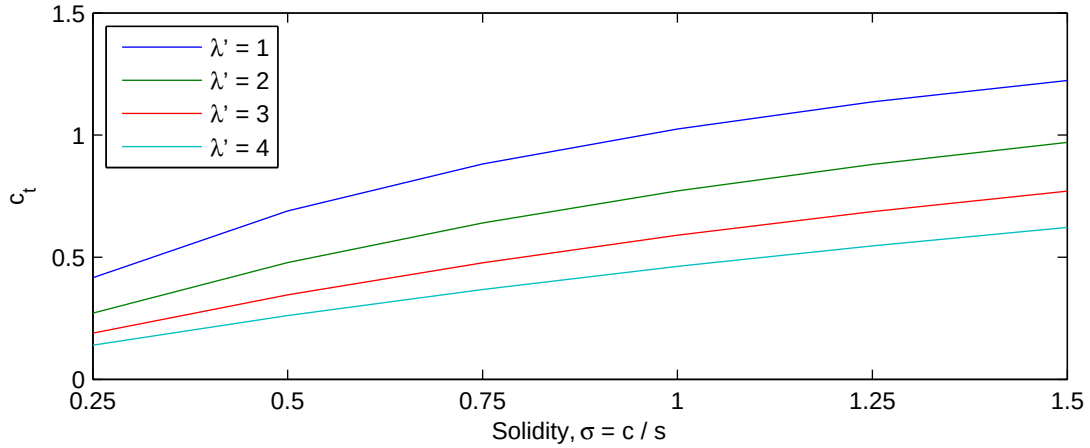

Figure 10: *Coefficient c_t versus solidity with varying blade speed ratios (and therefore stagger angles) for $\alpha' = 3°$.*

2.5 Hydrodynamic analysis as a low solidity turbine

The third analysis method considered is that commonly used for low solidity wind and tidal current turbines, whereby the blades are assumed to behave as if in isolation from each other, this meaning that section data for isolated aero/hydrofoils is used. As with the previous section, we again assume that the lift coefficient for a flat plate is given by $c_l = 2\pi \sin\alpha$, and that there is no flow-feedback.

It is known that this theoretical approach is unsuited to the current problem, but its use here, and the comparison with previous results, establishes a rough bound on the validity of low solidity theory for cases with higher solidity. It also provides for an independent (but approximate) cross-check of the previous results.

Figure 11 shows the variation in thrust coefficient with blade speed ratio for a number of different solidities and may be compared with Figure 9. The angle of incidence is 3° as before and a solidity of infinity again indicates that the analysis is as per Section 2.3.1/Figure 2. We see here that neglecting the effect of blade-blade interaction leads to an over-prediction of the thrust coefficient relative to the case for an effectively infinite solidity; indeed, only the results for a solidity of 0.25 show lower thrust coefficients across the range of blade speed ratios considered.

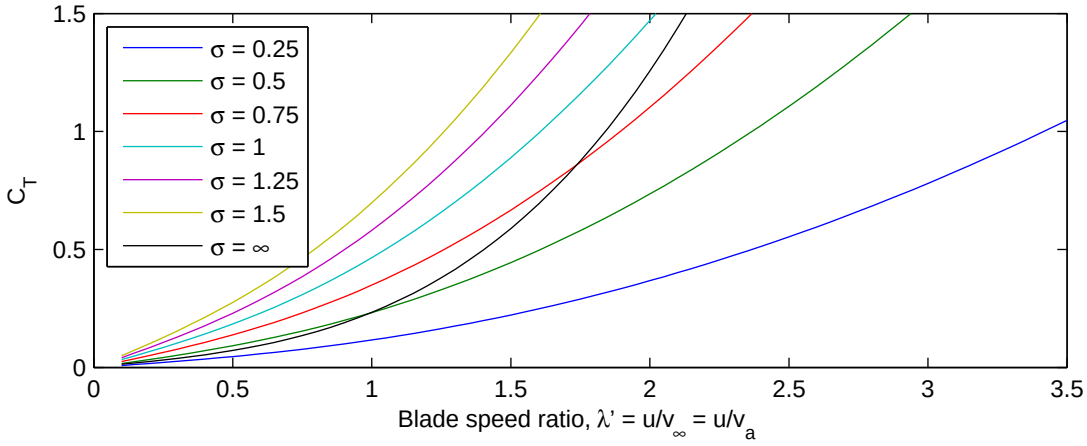

Figure 11: *Thrust coefficient versus blade speed ratio with varying solidity for $\alpha' = 3°$. $\sigma = \infty$ indicates the result which assumes no flow deviation.*

2.6 Consideration of the effect of ducting

Following discussion within the PerAWaT consortium, it was decided to use one of the ducts developed within WG3 WP1 to enclose the power take-off for the open-centre design, this being 'duct H'. This offers two key advantages: first, the present open-centre results may be directly compared with those for the ducted low solidity turbine which will be modelled in WG3 WP1; and second, there are results already available from WG3 WP1 for the behaviour of duct H with an actuator disc. These existing results for the duct can be used to assess how relevant the performance predictions of Section 2.3 (which considers an un-ducted device) are to the case of a ducted device by comparing C_T-a curves.

Such a comparison is achieved in the top graph of Figure 12 (the other graphs are included for interest). What is seen is that for thrust coefficients of between 0.4 and 0.6, this being the region of the design point for the present open-centre design, all of the different actuator disc configurations (bare and unbounded, bare and bounded, and ducted and bounded) result in similar values for the axial induction factor. Consequently, the flow angles will also be similar, and so the turbine should operate in a similar manner in a duct, as when bare (as was assumed in the design analysis). Thus, and to reiterate, this comparison strongly suggests that the open-centre turbine will behave similarly at the design point, and have the design point at a similar tip speed ratio, whether bare or ducted.

Away from the design point, or if the design point had a thrust coefficient lower than 0.4 or higher than 0.6, this is not the case, and the presence of the duct would result in a significantly different response to that predicted from unbounded actuator disc theory. For example, consider a turbine designed using actuator disc theory, with a design point thrust coefficient of 0.8 and tip speed ratio of 2. An axial induction factor of about 0.28 would be predicted, resulting in a local tip speed ratio (referenced to the axial velocity at the rotor plane) of $2/(1-0.28) = 2.78$. This point is labelled 'A' on Figure 13, which contains only the bare/unbounded and ducted/bounded results from the top graph of Figure 12.

If a duct were placed around this turbine, and if we assume briefly that the thrust coefficient is maintained, the axial induction factor would increase to about 0.43, this point labelled as 'B'. This would result in an increase in the local tip speed ratio, which would in turn case a decrease in the angle of attack. From the results of Figure 5, we know that this would then result in a decrease in the thrust coefficient, and so the operating point would move towards 'C'. What

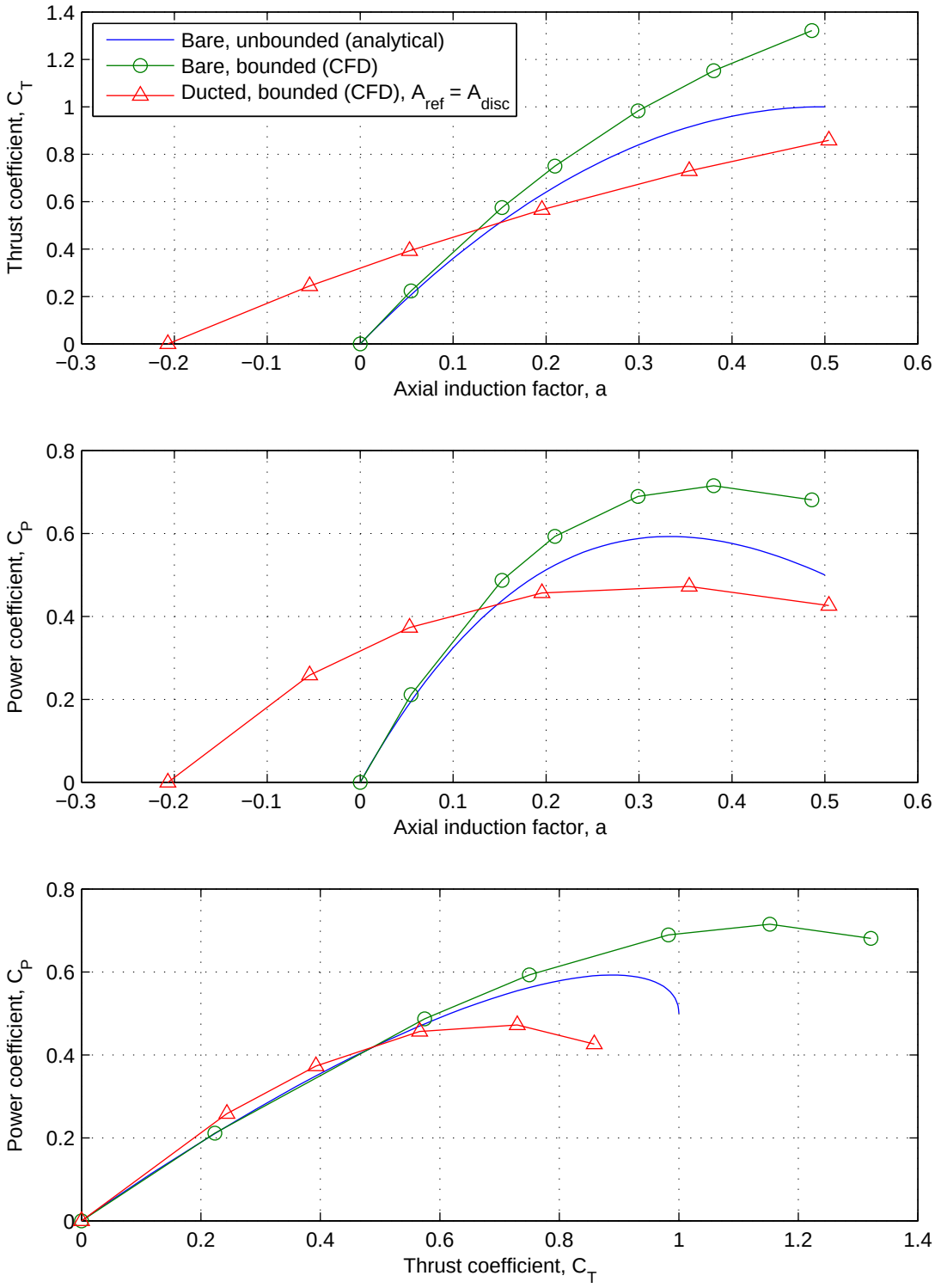

Figure 12: *Thrust and power coefficients versus axial induction factor, and the power coefficient versus the thrust coefficient, for analytical and CFD simulations of bare and ducted actuator discs. All CFD results are from WG3 WP1.*

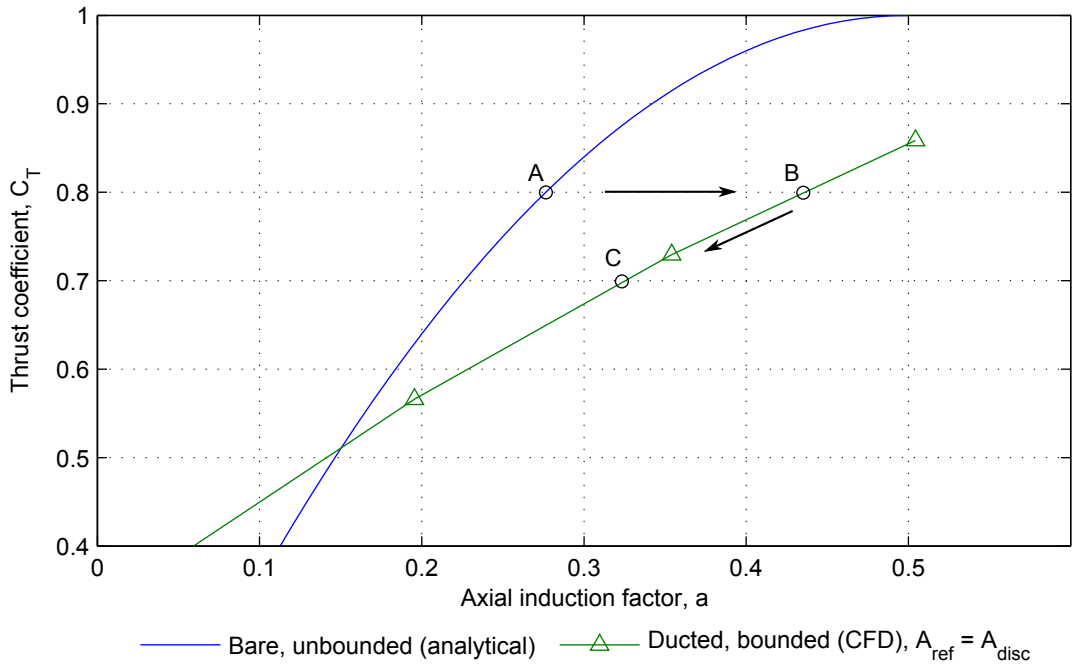

Figure 13: *Thrust coefficient versus axial induction factor for a bare and unbounded actuator disc, and for a ducted actuator disc in a bounded domain.*

is important, is that it is not known *a priori* where the new equilibrium point 'C' would be achieved (other than that both the thrust coefficient and the axial induction factor would be lower). Thus, we would no longer have confidence that the design tip speed ratio represented the optimum point of operation, as intended.[5]

2.7 Structural analysis

A basic structural analysis was conducted in order to determine a realistic thickness for the blades, which are assumed to be constructed from plate steel. It should be immediately highlighted that from a fluid dynamic perspective, the thickness of the blades is not thought to be a significant parameter and will thus not have a major bearing on the later CFD results for the turbine. Nevertheless, it was desired to add an element of physical realism to the design, hence this analysis.

The loading considered was that of the blades being exposed to a flow of 4 m/s normal to the chord, this being approximately the case when the rotor is not turning and is subject to the flow

[5]It is appreciated that this is a complex line of reasoning!

in a peak spring tide. A drag coefficient of 2 was assumed, this value being typical for a flat plate normal to the flow (see for example White, 1999). Given the fluid density, a loading per unit area can then be determined.

Two idealized structural configurations were considered: first, that of a beam cantilevered from one end, and second, that of a beam built in at both ends. This latter case is statically indeterminate and so a basic finite element analysis (FEA) package was used for the calculation. The reason for considering these two cases is that it is unclear (and impossible to determine without recourse to a full FEA analysis of the rotor) the extent to which the inner ring of the rotor will provide support to flap-wise bending. Note that in both cases the twist of the blade was not considered.

For the two cases, the predicted maximum bending moments were 175 kNm and 33 kNm. In order to produce a single value, these two estimates were simply averaged to give an approximate maximum bending moment of 100 kNm. Taking a typical yield stress for mild steel of 240 MPa (this value was used in the D1 report) and neglecting load and material factors suggests that a thickness of 35 mm is required. This value was also used for the inner ring of the rotor.

2.8 Conclusions from basic analysis

The analysis of the present section, especially that of Section 2.3.3, allows for the design of an open-centre turbine that is expected to achieve good power and thrust coefficients at the design point. The accuracy of these basic models will be evaluated from the subsequent CFD predictions, which will also predict the behaviour of the wake; something which the basic models of the current section cannot do.

Full details of the turbine geometry are given in Table 3, and two views of the 3D CAD model are shown in Figure 14. Note that for all radial positions on the blade between the inner and outer radius, the blade chord and twist are (linearly) interpolated from the values at the inner and outer radii.

Table 3: *Turbine geometry*

Parameter	Value
Duct outer diameter	18.0 m
Duct throat diameter	15.75 m
Duct length	18.0 m
Turbine outer diameter	15.75 m
Turbine inner diameter	7.875 m
Blade chord at outer diameter	3.093 m
Blade chord at inner diameter	1.546 m
Blade twist angle at outer diameter	17°
Blade twist angle at inner diameter	32°
Blade thickness	35 mm
Number of blades	16
Design tip speed ratio	2.5

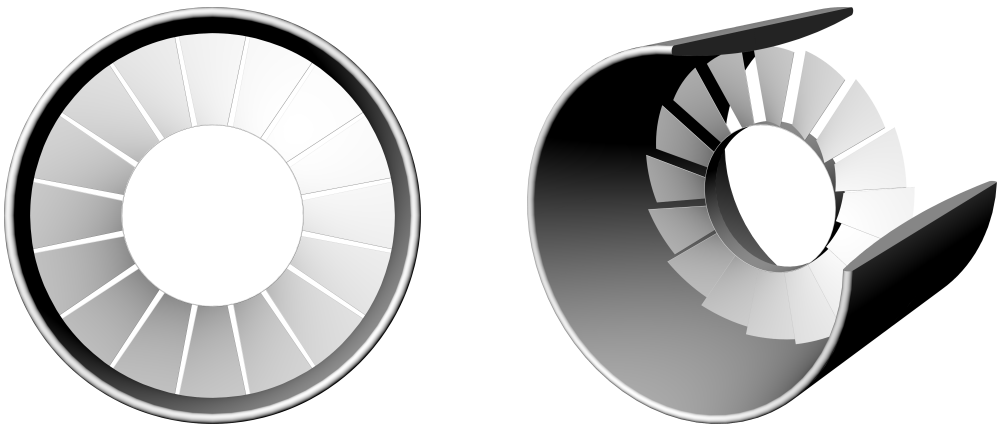

Figure 14: *Front (a) and isometric (b) views of the turbine with inner ring and duct.*

3 CFD simulations

3.1 Preliminary remarks

The general methodology for the current CFD simulations of the open-centre turbine closely follows that implemented for the generic (horizontal axis) turbine geometry for D1 of the current work package. In particular, the following salient features are noted to remain the same:

- A single blade is considered, and the model equations are the absolute velocity formulation of the RANS equations in a rotating frame of reference.

- As the open-centre turbine has 16 blades where the generic turbine has 3, the circumferential extent of the domain is now 22.5° as opposed to 120°.

- The axial extent of the domain is as before, extending 5 duct diameters upstream and 40 duct diameters downstream.

- The radial extent of the domain extends 4 duct radii from the axis of rotation. This was the value used for the tip speed ratio study of D1.

- All boundary conditions were as used previously, namely: specification of the velocity and turbulence quantities upstream and on the boundary at $r = r_{\max}$, a constant pressure condition on the downstream boundary, periodic conditions either 'side' of the domain segment, and no-slip walls on all other boundaries (either in the absolute or rotating domain, as appropriate).

One difference which might be highlighted here (for explanation) is that whereas in D1 the fluid volume modelled consisted of a straight, axial extrusion of the inlet plane, in the present work there is a 'dog-leg' in the vicinity of the rotor plane, as illustrated in Figures 15 and 24. This is introduced in order that the periodic boundaries are approximately positioned in the middle of the blade passages and therefore do not cut through the blades, and is standard practice in the analysis of axial-flow turbomachinery as it improves the robustness of the numerical solution.

3.2 Nomenclature

Table 4: *Nomenclature for the CFD analysis of the turbine.*

	Roman symbols
A_{ref}	Reference area used when calculating C_P and C_T. Unless otherwise noted the reference area is that of the disc/rotor for a bare turbine and that of the duct for a ducted turbine.
c_p	Pressure coefficient. Normalizing diameter varies. c_p = pressure/$(0.5\rho U_{\text{ref}}^2)$.
C_P	Power coefficient for the turbine, C_P = power/$(0.5\rho U_\infty^3 A_{\text{ref}})$.
C_T	Thrust coefficient for the turbine, C_T = axial force/$(0.5\rho U_\infty^2 A_{\text{ref}})$.
D	Diameter of the duct, unless otherwise noted
r	Radius
R	Radius of the duct, unless otherwise noted
U	Reynolds-averaged speed in the x-direction
U_∞	Freestream speed
x	Coordinate direction aligned with the axis of the turbine, with origin at the rotor plane and with the positive direction downstream
y	Coordinate direction aligned with the twist axis of the turbine blade modelled
z	Coordinate direction orthogonal to x and y
	Greek symbols
Δ_y	Distance from a solid wall in the wall normal direction
Δ_y^+	Non-dimensional distance from a solid wall in the wall normal direction
θ	Rotation angle. $\theta = 0$ is aligned with the y-axis.
λ	Tip speed ratio, also denoted TSR

3.3 Computational grid

3.3.1 Blocking strategy

The blocking strategy for the present case can be described by a series of operations, each effectively 2D in nature.

The first stage is to create a polar grid in the y-z/r-θ plane by collapsing the z-direction grid lines at the axis of rotation. This differs from the approach used previously and is due to the smaller circumferential extent of the domain.

The second stage is to create separate O-grids around the duct and inner ring of the turbine. These are in the r-x plane and extend through the complete circumferential extent of the domain.

The third and final fundamental step is to create an O-grid around the blade in the θ-x plane, extending from the inner surface of the duct to the outer surface of the inner ring.

Subsequent to these steps, a number of additional splits were introduced in order to target the grid cells towards the leading and trailing edges of the blade, duct and inner ring. Splits were also introduced to facilitate coarsening upstream and downstream of the turbine and towards the axis of symmetry. Note that the upstream and downstream coarsening started at $x/D = \pm 1$; this choice was based on further consideration of the results presented in the D1 report, where it had been concluded that coarsening from $x/D = 10$ downstream was the best choice. It is now believed that the minor differences in the predicted results (from grids with coarsening starting at $x/D = 1$ and $x/D = 10$ downstream) are unimportant in respect of the wake parameterization.

3.3.2 Grid spacing parameters

For the open-centre geometry, all grid spacings/cell counts were chosen to follow approximately those used for the generic turbine mesh, in order that there was a basic level of confidence in the present mesh with respect to grid verification.

Some representative wall-normal spacings are shown in Table 5, these having been determined from flat-plate boundary layer theory (e.g. White, 1999). As is seen, the mesh is designed to fully resolve the boundary layer on the blade (with a target Δ_y^+ value of 5), while wall laws will be used to represent the boundary layers on the duct and the inner ring (the exact determination of which is less important). At the junction of the blade with the duct and the inner ring the wall normal spacing is also increased in order to reduce the potential for highly skewed cells due to small geometric discrepancies. Comparing the blade spacings used here with those for the generic turbine, it will be seen that they are very similar; thus, as these parameters were verified for the 2D blade sections, there is confidence that the parameters chosen here for the open-centre rotor are appropriate.

Chord-wise/stream-wise cell counts on the blade, duct and inner ring are 148, 372 and 196 respectively (all of these numbers applying for the complete O-grid); in comparison, 104 cells were used chord-wise for the generic turbine blade with 72 cells on the hub and nacelle. For the

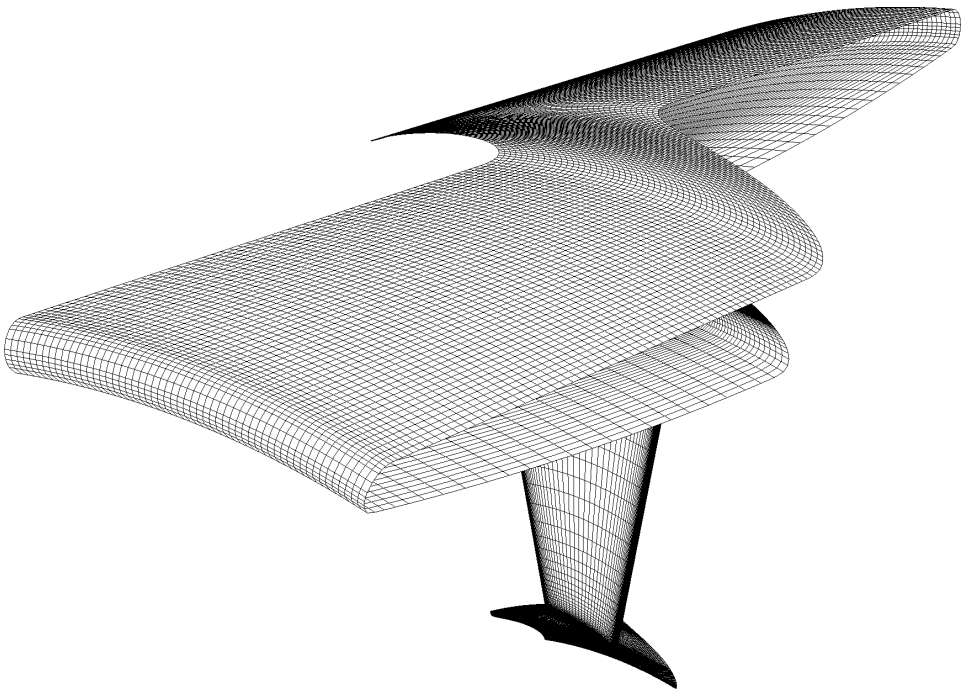

(a)

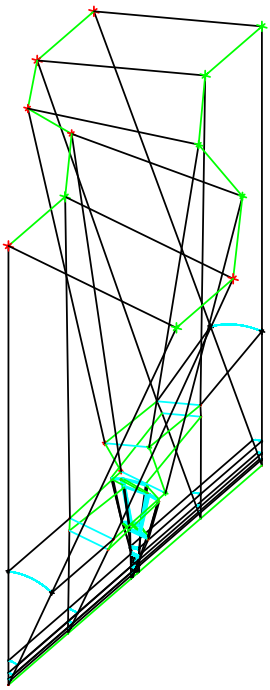

(b)

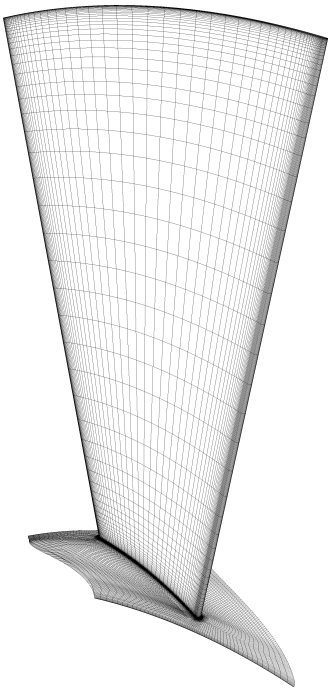

(c)

Figure 15: *Views of the mesh and blocking. a) shows the completed mesh on the duct, blade and inner ring while c) shows the mesh on the blade and inner ring only. b) shows the blocking in the vicinity of the turbine, with blocks upstream and downstream of $x/D = 1$ hidden. Note the dogleg in the domain in order that the periodic boundaries lie in the middle of a blade passage.*

Table 5: *Wall-normal spacings at various locations in the mesh*

Location	Δ_y (m)	Δ_y^+
Inner radius of blade	0.0002	25
Inner radius of blade, outside of inner ring boundary layer	4.0×10^{-5}	5
Outer radius of blade, outside of duct boundary layer	2.0×10^{-5}	5
Outer radius of blade	0.0004	100
Duct	0.001	100
Inner ring	0.0007	100

blade, the larger number of cells for the open-centre design is driven by the very small leading edge radius.

The span-wise cell count on the blade is 70, this comparing with the 92 cells used for the generic turbine. Fewer cells are used for the present case because the blade is shorter (relative to the chord) and because there is less span-wise variation in the geometry. Cell counts in the circumferential direction on the duct and inner ring are both 56. This number is largely dictated by the wall-normal spacing on the blade.

In total, and after coarsening of certain blocks as discussed in the section above, there are 2.0×10^6 cells in the mesh for the open-centre turbine. This compares with 1.5×10^6 cells for the comparable mesh for the generic turbine (same distance to the radial far-field boundary, and comparable coarsening). The primary reason for the larger number of cells (an approximately 40% increase) in the open-centre turbine mesh is the greater surface area of solid volume that must be meshed with small wall-normal grid spacings (this greater surface area being due to the presence of the duct and inner ring, in comparison to the hub and nacelle). As such, the open-centre turbine mesh is not 'finer' *per se*.

Given then the above similarities in grid spacings and cell counts between the present open-centre turbine mesh and the verified generic rotor mesh of D1, it is felt justified using the turbine mesh of D1 as a reference point with regards to grid verification, despite the somewhat different flow characteristics expected (and later observed).

3.4 Verification of the iterative convergence

Verification of the iterative convergence was achieved by monitoring the power and thrust coefficients, and the streamwise velocity component at a number of streamwise positions, all at $y/R = 0.5$ and $\theta = 0°$ (in line with the blade centreline). Graphs of these variables, as a function of the iteration number, are shown in Figures 16 and 17. These data are for three different tip speed ratios, being the lowest (2.2), middlemost (2.8), and highest (3.4).

Considering first the power and thrust coefficients, it is seen that convergence is achieved after 2000 iterations for all tip speed ratios, but that convergence is more rapid for the higher tip speed ratio cases. This is consistent with the fact that the power and thrust coefficients are lower for the higher tip speed ratio cases, which in turn means that the wake deficit velocities are lower, this resulting in a smaller departure from the initial conditions. In comparison with the results presented in the D1 report for the generic turbine (where convergence was achieved after 1000 iterations), the rate of convergence is clearly lower for the open-centre turbine. This was not investigated further as it does not affect the ultimate converged value.

Turning to the convergence of the streamwise velocity, Figure 17, there are two features in

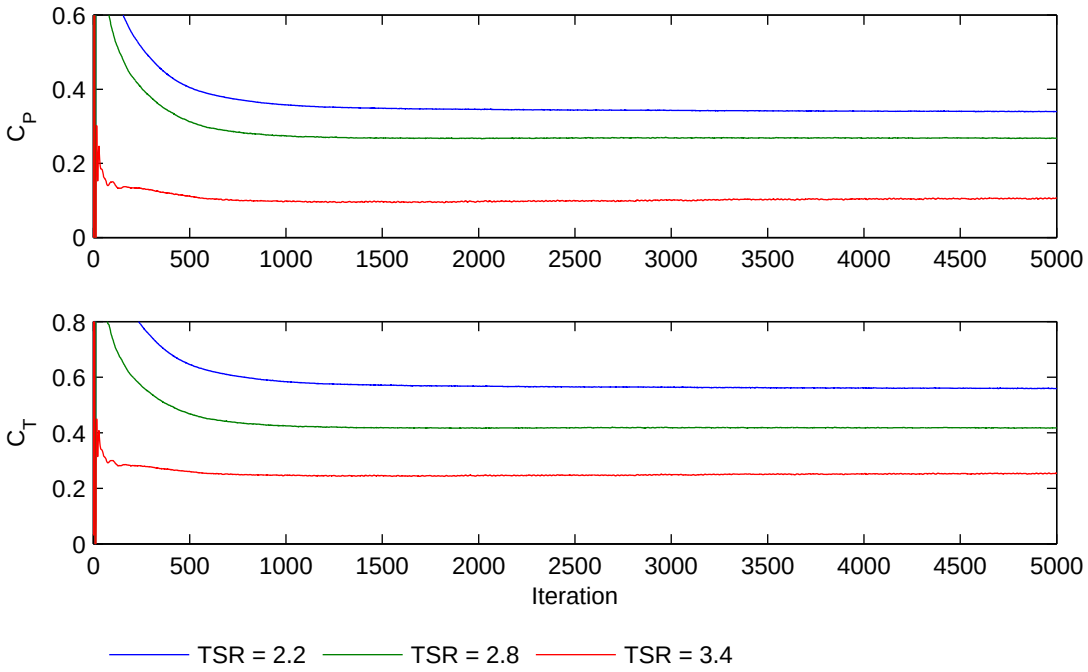

Figure 16: *Iterative convergence of the power and thrust coefficients for three different tip speed ratios.*

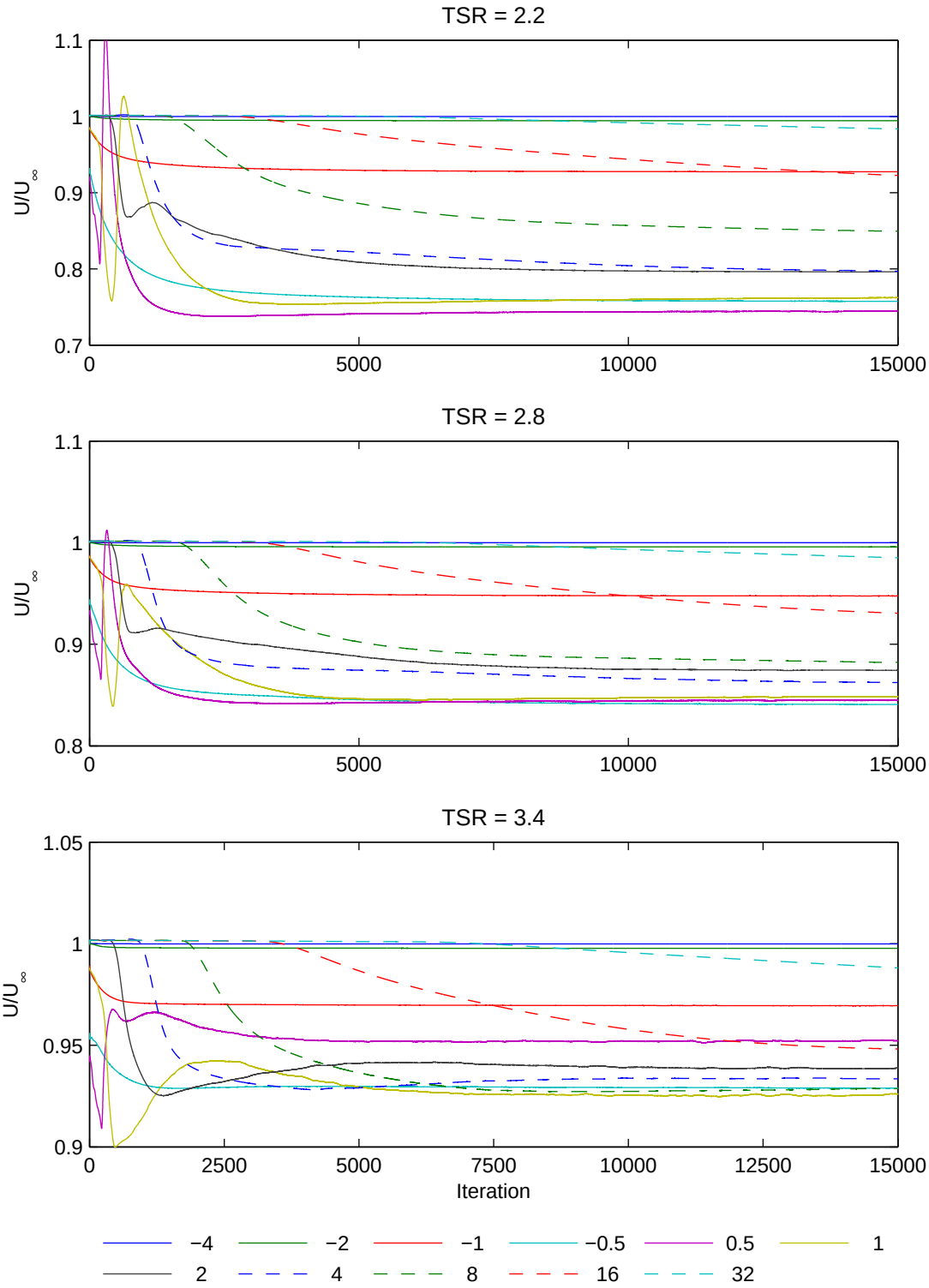

Figure 17: *Iterative convergence of the streamwise velocity component at a number of streamwise positions and for three different tip speed ratios. Note that the vertical scale varies in the three plots.*

common with the convergence of the power and thrust coefficients: first, convergence is more rapid for the higher tip speed ratio cases, and second, in comparison with the results for the generic turbine, convergence is again significantly slower. It is judged that for the highest tip speed ratio case ($\lambda = 3.4$), convergence is effectively complete for all points other than 32 duct diameters downstream, while for the lowest tip speed ratio case ($\lambda = 2.2$), convergence is not fully achieved for the two positions 16 and 32 diameters downstream. That all points up to 8 diameters downstream are converged for all tip speed ratios provides sufficient information for a parameterization to be carried out, and so the solutions were not advanced beyond the 15 000 iterations shown given the significant computational cost.

3.5 Parametric study of the tip speed ratio

The study of the tip speed ratio considered values between 2.2 and 3.4 with an increment of 0.2. A solution was also attempted for a tip speed ratio of 2.0 but this led to a failure of the solver. This failure was very likely due to the presence of massively-separated flow which cannot be handled with the current simulation setup (a steady state RANS solution). Instead, either an unsteady RANS simulation or potentially a Large Eddy Simulation would be required here. Neither of these were considered as massively-separated flow would lead to very poor turbine performance, and it is not the object of the present study to consider this.

Presentation of the results from this study is in the same format as the presentation of results for the generic turbine in the D1 report, in order to facilitate cross-comparison of different turbine technologies – one of the key objectives of the PerAWaT project. We thus consider the power and thrust coefficients, and longitudinal and lateral profiles of the streamwise velocity (Figures 18–21). Further analysis is provided in the form of pressure profiles on the blade and contour plots of the pressure on the blade and the flow speed on a plane within the fluid volume.

For the power and thrust coefficients, Figure 18, one trend which can be immediately highlighted is that both coefficients decrease monotonically with an increase in the tip speed ratio; this is the opposite trend to that generally observed for low solidity turbines, but is as expected from the basic analysis. We also see that the optimum C_P occurs immediately prior to blade stall; again, based on the data for flat plates, this is as expected. For practical operation in a turbulent environment, the desired operation point would be at a slightly higher tip speed ratio: most likely around 2.6. In comparison with the results for the generic turbine, significantly

lower C_P values are seen; this is due at least in part to the non-dimensionalization used, with the frontal area of the duct being used as a reference.

In Figure 19 we compare the present results for C_P versus C_T with the results from WG3 WP1 for an actuator disc in duct H, as already presented in Figure 12. There are two inconsistencies to note in this comparison: first, the blockage ratios are slightly different (6.25% for the present CFD work, 8.4% in the work from WG3 WP1); and second, the results from WG3 WP1 are for an actuator disc without a hole in the centre. The latter of these differences is expected to be the most significant. Thus, the only conclusion that can be drawn from the comparison is that the present CFD results lie on the correct side of the curve for the full actuator disc.

Figure 20 shows longitudinal profiles of the streamwise velocity at various lateral positions. Given the nature of the open-centre design, with the jet through the centre, it is difficult to offer much direct interpretation of these graphs and it is more instructive to look at the lateral profiles of the streamwise velocity, Figure 21. (Figure 20 is included here in order to allow cross-comparison with the generic turbine results of D1.) Turning therefore to these lateral profiles it is immediately apparent that the wake profiles are much more complex than for the generic turbine. Two salient features may be immediately highlighted: first, the deficit

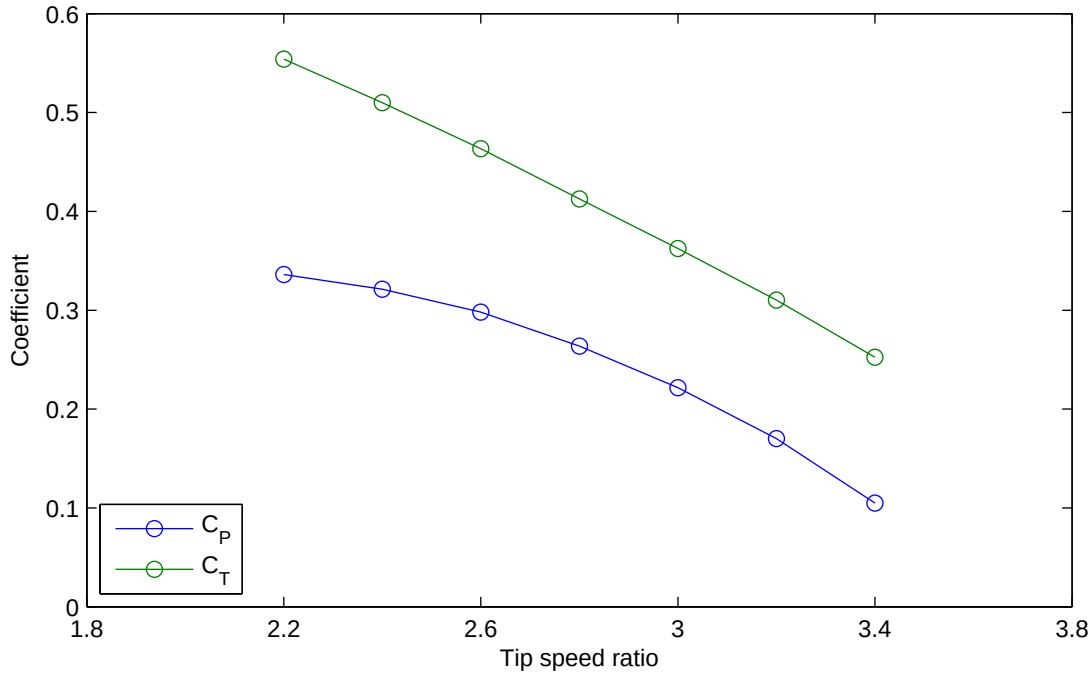

Figure 18: *C_P and C_T versus tip speed ratio.*

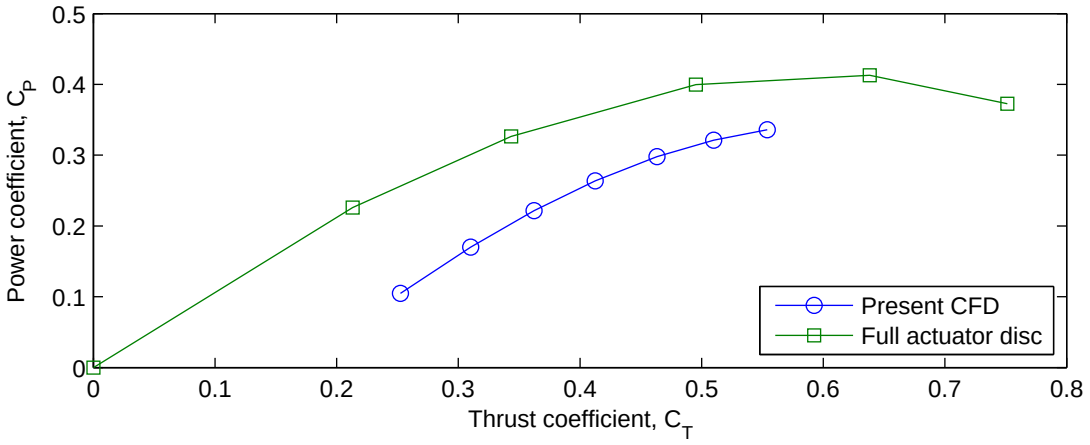

Figure 19: *C_P versus C_T from the present results and WG3 WP1 (cf. Figure 12).*

velocity is much lower, this being a direct result of the lower thrust coefficients produced for this turbine; and second, the maximum deficit velocity clearly occurs at the outer radius of the turbine (see especially the profiles at $x/D = 0.5$ and 1.0). As the wake develops, the position of the maximum deficit velocity moves towards the centreline as there is stronger mixing from the outer radius, due to the larger velocity gradient and the larger surface area for mixing.

It is also seen that the wake is still not fully developed (in the sense of a single, axi-symmetric wake about a centreline) at the last downstream position, $x/D = 16.0$. In consideration of this trend, we can see from the longitudinal profiles that the centreline deficit velocity does indeed increase downstream of the turbine; the opposite trend to that seen for the generic turbine. This is due to the presence of the central jet/bypass flow in the case of the open-centre turbine.

Pressure profiles on the blade were plotted in order to develop an understanding of the flow around the blade, as shown in Figure 23. In each of these plots the pressure is normalized using the maximum value of the pressure on the blade, this occurring at the leading edge stagnation point. This is equivalent to normalizing using the relative flow speed seen by the blade, a value which cannot be directly determined from the velocity field. Note also that the ordinate axis is reversed, following the convention for foil sections.

What is seen is that for the highest tip speed ratio the minimum value of the suction peak is approximately equal on the suction and pressure surfaces, indicating that the angle of attack is relatively small. For the lower tip speed ratios there is an increasing difference in these values, indicating an increasing angle of attack. Given the lack of experimental or alternative numerical data for pressure profiles on flat plate cascades or indeed flat plates it is difficult to

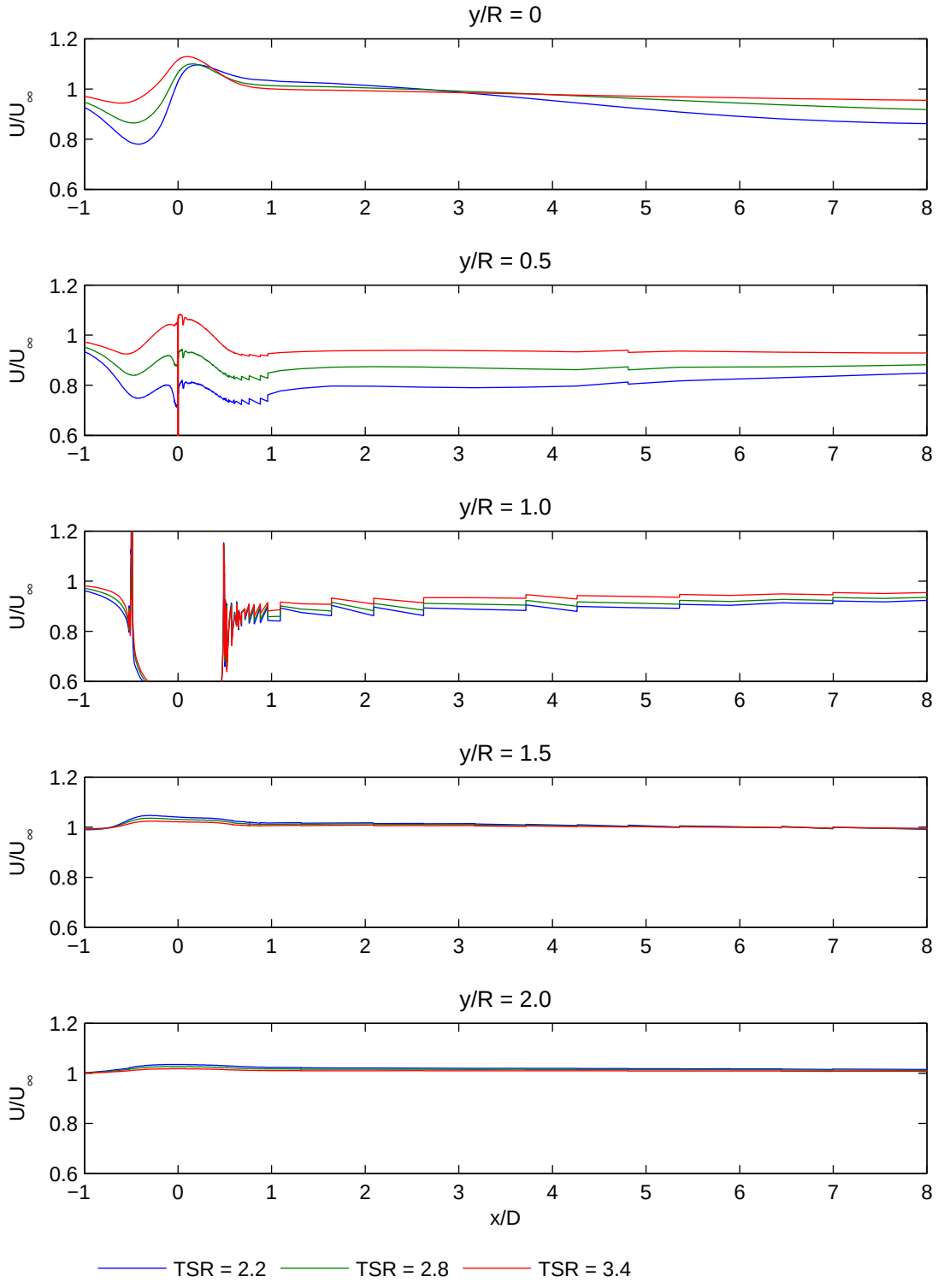

Figure 20: *Longitudinal profiles of the streamwise velocity at five lateral positions after 15 000 iterations. Breaks in the profiles are due to the presence of volumes outside of the fluid domain, while the stepped nature of the profiles is due to the fact that zeroth order interpolation is used. Note that the streamwise distance x is non-dimensionalized with respect to the duct diameter D whereas the transverse distance y is non-dimensionalized with respect to the duct radius R.*

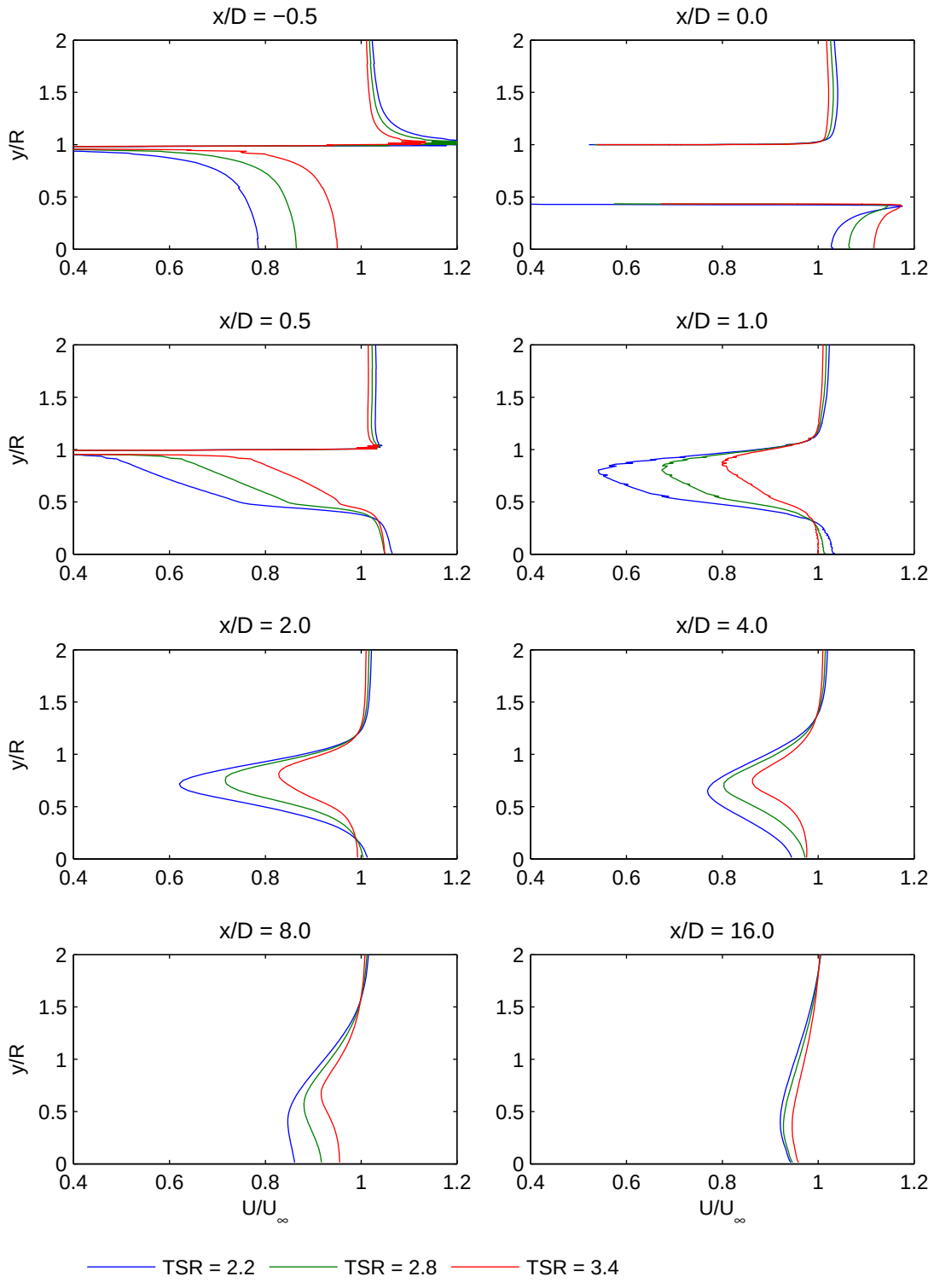

Figure 21: *Lateral profiles of the streamwise velocity at eight longitudinal positions after 15 000 iterations.*

assess whether these profiles are physically realistic. The only reference point which can be readily offered is that of a NACA 0006 aerofoil, Figure 22. At an angle of attack of 4°, the minimum pressure predicted by Xfoil (Drela and Youngren, 2001) is -3.2 whereas the angle of stall (from Abbott and von Doenhoff, 1959) is approximately 8°. The pressure profile from Xfoil is seen to be similarly 'peaky'. Thus, and in an approximate way, this suggests that the present results, especially given the cascade effect, are physically plausible.

Finally, in order to give a general indication of the flow field in the vicinity of the turbine, Figure 24 shows contour plots of the pressure coefficient on the turbine blade and inner ring, and the speed ratio on an *X*-*Z* plane at the mid-span of the blade. This shows the rapid changes in the pressure around the leading edge of the blade, as shown previously in Figure 23, and also the accompanying accelerations of the flow near the blade.

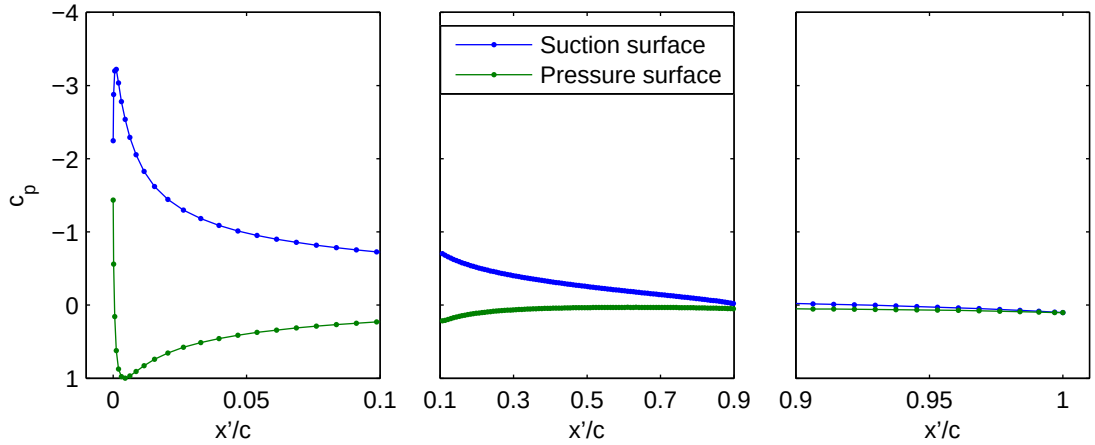

Figure 22: *Pressure profile on a NACA 0006 foil at an angle of attack of 4°, a Reynolds number of 3×10^6, and with forced transition. As with Figure 23, the direction of the ordinate axis is reversed.*

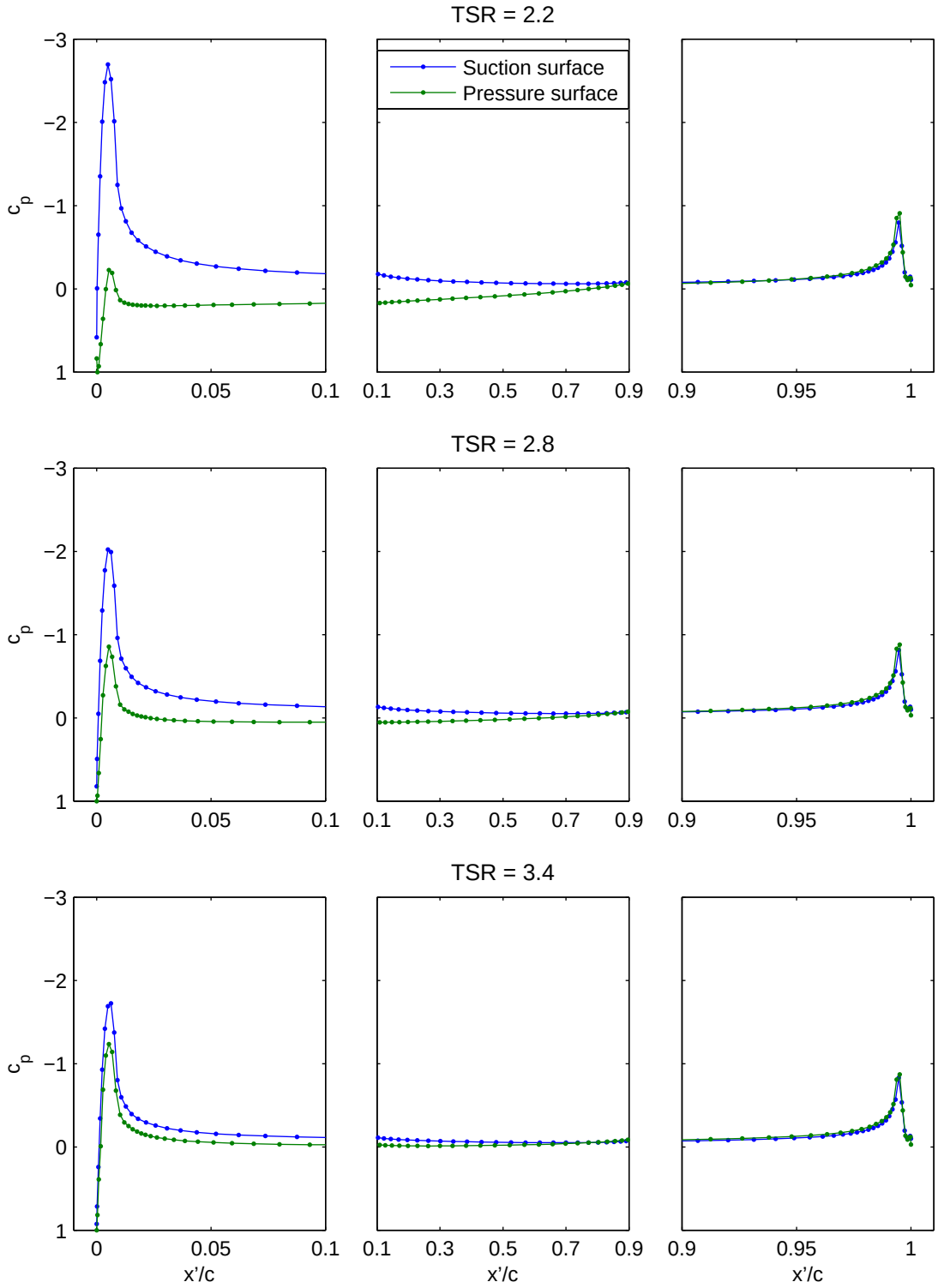

Figure 23: *Pressure profiles on the blade at mid-span after 15 000 iterations. The coordinate direction x′ is aligned with the chord of the blade and is zero at the leading edge. For these plots the pressure is normalized using the maximum value of the pressure on the blade, i.e. that at the leading edge stagnation point. Note also that the direction of the ordinate axis is reversed.*

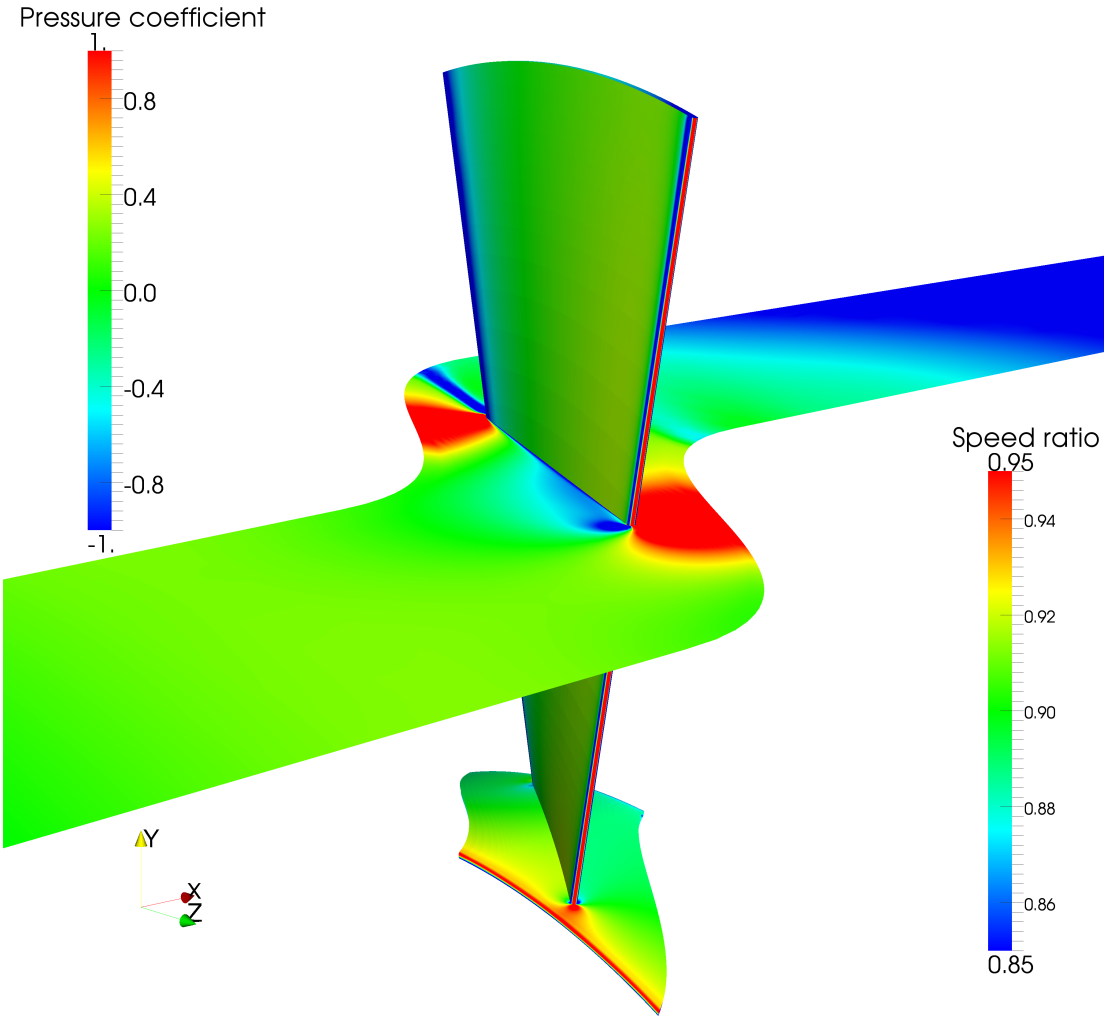

Figure 24: *Contour plots of the pressure coefficient on the blade (normalized using the free stream speed) and the speed ratio (in the stationary frame) on a plane at mid-span of the blade (also normalized using the free stream speed) at a tip speed ratio of 2.8 and after 15 000 iterations.*

4 Conclusions

This report introduces a novel analytical model for a high solidity tidal current turbine, being a fusion of the modelling approaches normally applied to high solidity axial-flow turbomachines and low solidity wind and tidal current turbines. One of the immediate predictions from this model is that the thrust coefficient will *decrease* with the tip speed ratio, this being the opposite qualitative trend to that generally seen for low solidity turbines. This is due to the fact that for high solidity turbines all of the flow through the rotor plane follows the blade angle, irrespective of the tip speed ratio, whereas for low solidity turbines this depends strongly on the tip speed ratio.

Based on the results from this analytical model, a credible design for a high-solidity rotor is arrived at. A basic structural analysis was also conducted in order to arrive at a plausible blade thickness, although, as stated, it is not thought that the hydrodynamics of the rotor will be strongly dependent on this. Finally, the geometry for the generator housing is chosen to be that of duct H from the work in WG3 WP1, with results from this work package showing that the response of a ducted turbine at the design point (where response refers to the axial induction factor) is similar to that of an un-ducted rotor.

The CFD predictions from the second part of this report, which take as their input the afore-mentioned design, confirm that the trend of C_T decreasing with tip speed ratio, predicted by the basic analytical model, is correct. The CFD simulations also give a prediction for the power coefficient, which was not given by the basic analytical model. Longitudinal and lateral profiles of the streamwise velocity show that the wake is significantly more complex than that produced by a turbine without an open-centre. This is because the turbine produces an annular deficit region, rather than an essentially disc shaped deficit region, and because there is mixing of this deficit region from both the inner jet produced by the open-centre and the outer perimeter.

In comparison with the results from D1, it is seen that for the near wake, the deficit velocities are lower, due to the lower thrust coefficients, and that the greatest deficit occurs towards the outer radius. For the far wake, it is observed that the position of maximum deficit velocity moves towards the axis of rotation, and that the centreline velocity deficit increases as the wake develops. This latter fact is because at the rotor plane the centreline velocity is that of the jet through the open-centre and therefore not in the ‘wake’ of the turbine.

A key sensitivity of the present analytical and CFD modelling is the ability to accurately model cases where the angle of attack is high. This is indeed a sensitivity of all turbine modelling, such as that presented in the D1 report for a low solidity axial-flow turbine, but is thought to be especially important for the current case where the blades are formed from flat plates. In the analytical modelling of Section 2.3, which is used as the basis of the current design, this problem is addressed by limiting the angle of attack to 5°, such that only realistic results are produced. For the CFD modelling of Section 3 the angle of attack is not known *a priori* and cannot be readily determined from the results. Based though on the pressure profiles of Figure 23, there is a good level of confidence that for the medium to high tip speed ratios considered the angle of attack will be small and therefore the results will be valid. Further to this, given the trend in the C_P- and C_T-λ curves shown in Figure 18, the results for lower tip speed ratios also appear plausible (with respect to the higher tip speed ratio results).

5 Acceptance criteria

The acceptance criteria for the present deliverable (as amended in Variation Request 11) are as follows:

1. Model will include:
   (a) Geometry of the moving rotor and any rotating, hydrodynamically active surfaces
   (b) Model designed for prototype scale (as defined in WG0) in a typical water depth (defined in WG0) with no waves.
   (c) Grid converged quality assured models generated (the point at which your results are no longer statistically varying)
   (d) The model will exploit the rotational symmetry of the turbine and utilize periodic boundary conditions.
2. Report will include:
   (a) Description of model methodology including all algorithms and assumptions
   (b) Wake described with sufficient detail to allow a parameterization to be made.
   (c) Assessment of model performance via comparison with data from WG3 WP1
   (d) Discussion of sensitivities and limitations.

With respect to point 1a), the model includes the blade and inner ring as well as the stationary duct; this latter part being additional to the acceptance criteria. As regards point 1b), it may be noted that this report includes a significant level of design work beyond that anticipated. In respect of the criteria for "grid converged quality assured models", this is provided by reference to the grid spacings in the D1 report (see in particular Section 3.3.2 of the present report); convergence in time is demonstrated in Section 3.4. As discussed in Section 3.1, the model exploits the rotational symmetry of the turbine and therefore used periodic boundary conditions.

Turning to the report acceptance criteria, the model methodology is as per the D1 report and so reference is here made to this previous report; this is also the case in respect of the fidelity of the wake. Comparisons with the results of WG3 WP1 are provided where possible i.e. in the final conclusions; it is also the case that results from WG3 WP1 were used to define the duct of the existing model.[6] A discussion of the sensitivities and limitations of the model is provided throughout Section 3.5 and again in the final conclusions.

[6]It is the intention to provide full comparisons between models in the D4 report, by which time the appropriate results will be available from WG3 WP1. This small timetabling discrepancy has no knock-on effects and will be addressed in a variation request which is in preparation.

References

Abbott, I. H. and von Doenhoff, A. E. (1959), *Theory of Wing Sections*, Dover.

Burton, T., Sharpe, D., Jenkins, N., and Bossanyi, E. (2001), *Wind Energy Handbook*, Wiley.

Drela, M. and Youngren, H. (2001), *Xfoil 6.9 User Primer*.
URL `http://web.mit.edu/drela/Public/web/xfoil/`

Fage, A. and Johansen, F. C. (1927), On the flow of air behind an inclined flat plate of infinite span, *Proceedings of the Royal Society of London: Series A*, 116(773), pp. 170–179.

Hoerner, S. F. (1985), *Fluid-Dynamic Lift*, 2nd edition.

Japikse, D. and Baines, N. C. (1994), *Introduction to Turbomachinery*, Concepts ETI, Inc. and Oxford University Press.

Johnson, I. A. and Bullock, R. O. (eds.) (1965), *Aerodynamic design of axial flow compressors*, NASA, SP-36.

Sabersky, R. H., Acosta, A. J., Hauptmann, E. G., and Gates, E. M. (1999), *Fluid Flow*, Prentice Hall, 4th edition.

White, F. M. (1999), *Fluid Mechanics*, McGraw-Hill, 4th edition, (International edition).

Wislicenus, G. F. (1947), *Fluid Mechanics of Turbomachinery*, McGraw-Hill, 1st edition.